Since January 2020 Elsevier has created a COVID-19 resource centre with free information in English and Mandarin on the novel coronavirus COVID-19. The COVID-19 resource centre is hosted on Elsevier Connect, the company's public news and information website.

International Journal of Biological Macromolecules 219 (2022) 694–708

Contents lists available at ScienceDirect

International Journal of Biological Macromolecules

journal homepage: www.elsevier.com/locate/ijbiomac

Engineering alginate hydrogel films with poly (3-hydroxybutyrate-*co*-3-valerate) and graphene nanoplatelets: Enhancement of antiviral activity, cell adhesion and electroactive properties

Alejandro Hurtado [a], Alba Cano-Vicent [a], Alberto Tuñón-Molina [a], Jose Luis Aparicio-Collado [b], Beatriz Salesa [a], Roser Sabater i Serra [b,c,*], Ángel Serrano-Aroca [a,*]

[a] *Biomaterials and Bioengineering Lab, Centro de Investigación Traslacional San Alberto Magno, Universidad Católica de Valencia San Vicente Mártir, c/Guillem de Castro 94, Valencia 46001, Spain*

[b] *Centre for Biomaterials and Tissue Engineering, Universitat Politècnica de València, 46022 València, Spain*

[c] *CIBER-BBN, Biomedical Research Networking Centre in Bioengineering, Biomaterials and Nanomedicine, 46022 València, Spain*

ARTICLE INFO

Keywords:
PHBV
Alginate
Graphene nanoplatelets

ABSTRACT

A new biodegradable semi-interpenetrated polymer network (semi-IPN) of two US Food and Drug Administration approved materials, poly(3-hydroxybutyrate-*co*-3-valerate) (PHBV) and calcium alginate (CA) was engineered to provide an alternative strategy to enhance the poor adhesion properties of CA. The synthesis procedure allows the additional incorporation of 10 % *w/w* of graphene nanoplatelets (GNPs), which have no cytotoxic effect on human keratinocytes. This quantity of multilayer graphene provides superior antiviral activity to the novel semi-IPN against a surrogate virus of SARS-CoV-2. Adding GNPs hardly affects the water absorption or electrical conductivity of the pure components of CA and PHBV. However, the semi-IPN's electrical conductivity increases dramatically after adding GNP due to molecular rearrangements of the intertwined polymer chains that continuously distribute the GNP nanosheets, This new hydrophilic composite biomaterial film shows great promise for skin biomedical applications, especially those that require antiviral and/or biodegradable electro-conductive materials.

1. Introduction

Semi-interpenetrated polymer networks (semi-IPNs), consisting of a mixture of two polymers in which only one is crosslinked [1,2], are an advanced method of generating composite biomaterials with enhanced biomedical properties [3]. Biopolymers of natural origin such as alginate [4] or poly (3-hydroxybutirate-*co*-3-hydroxyvalerate) (PHBV) [5] can be used to make new biocompatible and biodegradable materials essential for a broad range of biomedical applications. The current SARS-CoV-2 pandemic has made scientists to focus their research activities on using materials with intrinsic antimicrobial properties, such as calcium alginate [6,7] and carbon-based nanomaterials (CBNs) [8], or hybrid biomaterials composed of CBNs in combination with biodegradable polymers such as alginate [4,9–12] or PHBV [13–15]. CBNs are highly promising materials, since they are capable of inactivating a broad range of microorganisms and can induce tissue regeneration [8,16]. Furthermore, they are characterized by a low risk of microbial resistance and when added to biomaterials they improve not only the antimicrobial properties but also other physical properties, such as mechanical performance, thermal properties, water diffusion, wettability and electrical conductivity [17–20].

Alginate and PHBV are US Food and Drug Administration biomaterials of natural origin that can be obtained from different types of microorganisms [21–24]. Alginate can also be extracted from brown algae [25]. PHBV is a biocompatible material with little or no cytotoxicity [23] but due to its high cost it is currently promising only for

* Correspondence to: Correspondence to R.S. i Serra, Center for Biomaterials and Tissue Engineering, Universitat Politècnica de València, 46022 València, Spain, and Á. S.A., Biomaterials and Bioengineering Lab, Centro de Investigación Traslacional San Alberto Magno, Universidad Católica de Valencia San Vicente Mártir, c/ Guillem de Castro 94, Valencia 46001, Spain.

E-mail addresses: rsabater@die.upv.es (R.S. i Serra), angel.serrano@ucv.es (Á. Serrano-Aroca).

https://doi.org/10.1016/j.ijbiomac.2022.08.039
Received 4 June 2022; Received in revised form 30 July 2022; Accepted 7 August 2022
Available online 10 August 2022

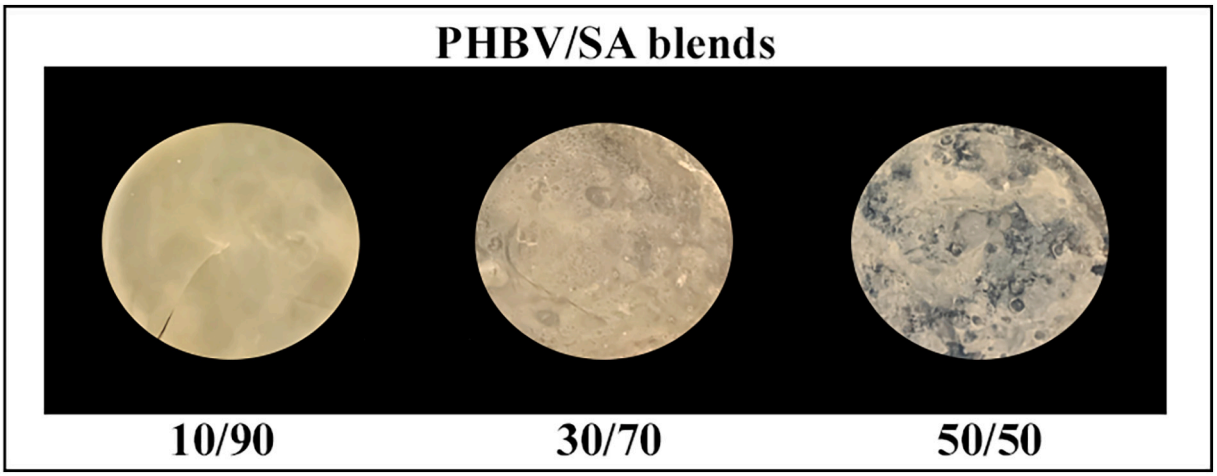

Fig. 1. Films of poly (3-hydroxybutirate-*co*-3-hydroxyvalerate)/sodium alginate (PHBV/SA) blends.

biomedical applications [14,26]. Some of its drawbacks are its low water absorption due to its high hydrophobicity. It is also more brittle than other materials and has low biological activity and null antimicrobial activity [14]. PHBV's physical and biological properties can be improved by adding CBNs [5,14]. PHBV has many potential biomedical applications, such as absorbable surgical sutures, drug delivery matrices and tissue engineering applications [14,27,28]. Combining PHBV with a significant percentage of graphene can produce composites with conductive properties for different applications in the biomedical field that require electrical stimulation [29].

Alginates are biocompatible materials with a molecular structure composed of β-D-mannuronic acid (M) and α-L-guluronic acid (G) blocks, which are linked by 1, 4- O-glycosidic bonds [24,30]. The G blocks are those involved in the gelation process, the stability of the alginate structure and the mechanical properties [24,31], so that alginates with higher viscosity and lower flexibility are generated when the concentration of G blocks is high. Crosslinking with divalent cations, such as Ca^{2+}, Zn^{2+} or Mg^{+2}, is essential for the formation of hydrogels with the typical egg-box structure [32]. Alginate hydrogels can absorb large amounts of water without being dissolved [4], although their cell adhesion on alginate substrates has been reported to be very poor [5,33].

Graphene is a bidimensional material with very high electrical conductivity, excellent mechanical performance, good thermal stability and large specific area and is highly compatible with biological systems [34–38]. Multi-layer graphene (2–10 layers), also called graphene nanoplatelets (GNPs), has shown significant proliferative activity at non-toxic concentrations in human keratinocytes [39]. GNPs have shown capacity to induce the expression of six genes related to wound healing, which make them promising nanomaterials for skin tissue engineering.

In the present study we hypothesised that a new biomaterial composed of crosslinked alginate and PHBV in the form of semi-IPN would improve the cell adhesion of neat alginate. We also considered that incorporating graphene nanoplatelets into these semi-interpenetrated systems would produce a hydrophilic composite biomaterial with enhanced physical, chemical and biological properties for potential biomedical applications. The physical, chemical and biological properties of these semi-IPNs were studied in terms of water absorption at body temperature (37 °C), functional groups, thermal behaviour and degradation, electrical conductivity, opacity, cytotoxicity, antiviral activity and cell adhesion.

2. Materials and methods

2.1. Materials

Poly (3-hydroxybutirate-*co*-3-hydroxyvalerate) (Sigma-Aldrich, Saint Louis, USA) revealed a previously a hydroxylvalerate copolymer mole ratio of 15.23 % by nuclear magnetic resonance [5]. Sodium alginate (SA, Sigma-Alrich, Saint Louis, USA) was previously characterized [40] as follows: Number average molecular mass (Mn) 60.5 ± 5.8 kDa, average molecular mass (Mw) 107.9 ± 2.7 kDa, and polydispersity (Mw/Mn) 1.79 ± 0.13; distribution of Guluronic (G) and Mannuronic (M) as FG = 0.436, FM = 0.564, FGG = 0.251, FGGG = 0.202. Calcium chloride (anhydrous, granular ≤7.0 *mm*, ≥93.0%) and graphene nanoplatelets with a surface area of 500 m^2/g were purchased from Sigma-Aldrich (Saint Louis, USA). The graphene nanoplatelets were previously characterized [39] as follows: Raman I_D/I_G value of 0.11; Dynamic light scattering (DLS) particle sizes of 625.8 nm and 2042 nm in water and in Dulbecco's modified Eagle medium (DMEM), respectively; Zeta potential from −38.6 mV to 2.69 mV according to the pH, ranging from 12 to 3, respectively. Dimethyl sulfoxide (DMSO) was provided by Fisher Bioreagents (Waltham, Massachusetts, USA) and chloroform (99,9 %, anhydrous max. 0,003 % H_2O, with molecular sieves, stabilized with 150 ppm of amylene) was supplied by Scharlau (Barcelona, Spain).

2.2. Film preparation

PHBV was mixed with sodium alginate in several weight ratios (100/0, 50/50, 30/70, 10/90, 0/100 PHBV/SA) to produce films by solvent casting [2]. PHBV was dissolved in 50 mL of chloroform at a concentration of 2 % *w/w* (1 g of PHBV dissolved in 50 mL of chloroform) at room temperature (25 ± 0.5 °C) under continuous stirring for 60 min in a gas extraction hood. SA was also dissolved in distilled water at a concentration of 2 % *w/v* (1 g of SA dissolved in 50 mL of distilled water) at 25 ± 0.5 °C under constant stirring for 30 min. After complete dissolution of the pure SA and PHBV polymers in their respective suitable solvents (chloroform and distilled water, respectively), they were placed in a glass Petri dish under a gas extraction hood at 25 ± 0.5 °C for at least 24 h to avoid sample cracking from fast drying, after which they were placed in a vacuum oven at 37 °C for 48 h to constant weight. The pure PHBV films (100/0 PHBV sample) and pure SA (0/100 PHBV/SA) were obtained after total evaporation of the solvents. The 50/50, 30/70, 10/90 PHBV/SA compositions were achieved by mixing the required volume of the 2 % *w/v* alginate/distilled water mixture with the required volume of a 2 % *w/v* PHBV/chloroform/DMSO mixture (with a chloroform/DMSO ratio of 60/40 *v/v*, 15 mL of chloroform and 10 mL of

Table 1
Notation used for the new material films developed and control films.

Identification	Material description
SA	Sodium alginate (without crosslinking)
SA 10G	Sodium alginate with 10 % *w/w* of GNPs
CA	Sodium alginate crosslinked with divalent cations of calcium (calcium alginate)
CA 10G	Calcium alginate with 10 % *w/w* of GNPs
PHBV	Poly(3-hidroxybutyrate-*co*-3-valerate)
PHBV 10G	Poly(3-hidroxybutyrate-co-3-valerate) with 10 % *w/w* of GNPs
PHBV/SA 10/90	Mixture of 10 % *w/w* PHBV and 90 % *w/w* of SA
PHBV/SA 10/90 10G	Mixture of 10 % *w/w* PHBV and 90 % *w/w* of SA with 10 % *w/w* of GNPs
PHBV/CA 10/90	Semi-IPN of 10 % *w/w* PHBV and 90 % *w/w* CA
PHBV/CA 10/90 10G	Semi-IPN of 10 % *w/w* PHBV and 90 % *w/w* CA with 10 % *w/w* of GNPs

DMSO) under magnetic stirring for 1 h at 25 ± 0.5 °C and subsequently a total mixture volume of 50 mL were placed in Petri dishes. The PHBV/chloroform/DMSO mixture was prepared with a first step of dissolving 1 g of PHBV in 15 mL of chloroform under stirring for 1 h under a gas extraction hood at 25 ± 0.5 °C until complete dissolution. The second step consisted of adding 10 mL of DMSO to the previous PHBV/chloroform solution and subjecting the mixture to continuous stirring for 20 min. The optimal chloroform/DMSO ratio of 60/40 *v/v* was determined experimentally to obtain a homogeneous mixture of both polymers (PHBV and SA) with different chemical behaviours (hydrophobic/hydrophilic, respectively). The final PHBV/SA 50/50, 30/70, 10/90 films were obtained after solvent evaporation under a gas extraction hood at 25 ± 0.5 °C for at least 24 h to avoid sample cracking from fast drying, followed by placing them in a vacuum oven at 37 °C for 48 h to constant weight. After analysing all the blend films, PHBV/SA 10/90 films were selected for being the most homogeneous (Fig. 1) and this composition had the advantage of containing a low percentage of PHBV, the most expensive polymer.

SA pure films and PHBV/SA 10/90 blend films were crosslinked by immersing the films in a 2 % *w/v* calcium chloride aqueous solution (10 g of $CaCl_2$ dissolved in 500 mL of distilled water) for 2 h to produce films indissoluble in water [11,12]. After crosslinking SA chains, the films were washed three times with distilled water and dried at 25 ± 0.5 °C under a gas extraction hood for 24 h to avoid film cracking from rapid drying, and then in a vacuum oven at 37 °C to constant weight for about 48 h. PHBV films, alginate (both pure and crosslinked), and PHBV/alginate 10/90 (with and without crosslinking) were also prepared by adding1, 5 and 10 % *w/w* of GNPs (% with respect to the polymer mass) following the same protocol but dispersing the corresponding mass of GNPs in the respective solvents (distilled water, chloroform or the 60/40 chloroform/DMSO mixture) by sonication for 30 min before adding sodium alginate or PHBV or 10/90 PHBV/alginate mixture to the same beaker. After measuring the electrical conductivity (see Section 2.5.6.) of the PHBV/CA 10/90 films with 1, 5 and 10 % *w/w* of GNPs, the 10 % film was selected as the only one that showed a very high increase of electrical conductivity. Table 1 shows the notation used for the new material films developed, as well as the films used as control for the physical and chemical characterization and biological performance of the materials.

2.3. Purification and sterilisation

After synthesis, the films were cut in the form of 10 mm diameter discs and purified three times by washing in 100 mL of a 50/50 distilled water/absolute ethanol (VWR CHEMICALS, Pennsylvania, United States) mixture under constant stirring for 1 h at room temperature, after which each sample was washed again 3 times in distilled water for 10 min in the same stirring conditions. Finally, the samples were dried in an oven at 37 °C for 2 days. Samples used for biological characterization were then sterilised by a 12.0 W UV-C ultraviolet radiation (UV) lamp under a laminar flow hood for 2 h (1 h for each material disc face).

2.4. Biological characterization

2.4.1. Cytotoxicity and cell adhesion

Human keratinocyte HaCaT cells were provided by La Fe Research Institute and Hospital, Valencia, Spain. The cells were cultured at 37 °C in DMEM containing 10 % fetal bovine serum (FBS), 100 units/mL penicillin and 100 mg/mL streptomycin in a 5 % CO_2 incubator. The films' cytotoxicity was assessed according to the ISO 10993-5:2009 standard on the biological evaluation of medical devices. 3 cm^2/mL sterilised film discs ($n = 6$) were placed in a 12-well plate with 1 mL per well of DMEM without FBS and incubated in a humidified CO_2/air (5/95 %) atmosphere at 37 °C for 72 h. The film extracts were then collected and passed through a filter (0.20 μm) to be later used in the cytotoxicity tests. 96-well plates were used to culture the cells at a density of 5×10^5 cells/well. After 24 h of cell incubation, the medium present in each well was replaced with 100 μL of the film extracts. 100 μL of the medium used to produce the film extracts was used as positive control, and 100 μL of a toxic zinc chloride solution as negative control [41]. 5 mg/mL of 3-(4,5-dimethylthiazol-2-yl)-2,5-diphenyltetrazolium bromide (MTT) was used to incubate the cells in each well for 4 h and the formazan crystals were dissolved in 100 μL of DMSO at room temperature. A microplate reader (Varioskan, Thermo Fisher, USA) was used to measure the absorbance readings at 550 nm.

The cell adhesion study was performed by Fluorescence Microscopy [42] in a Motic BA410 ELITE Series microscope provided with a Complete EPI-Fluorescence Kit Motic on the HaCaT human keratinocyte cell line. Sterilised films were hydrated with 0.5 mL DMEM without FBS in a 24 multi-well plate (1 disc/well) for 30 min.

A preliminary test was performed to determine the optimal cell concentration on three circular glass coverslip controls, after which 8.5×10^5 cells/well were seeded onto the different film surfaces. Cells were also seeded onto round glass coverslips (control surfaces). After 24 h, 48 and 72 h of incubation, each well was rinsed with PBS and fixed with PFA (4 %), Triton X-100 (0,1 %) in PBS and FBS (10 %) in PBS. The cells were stained with DAPI (Sigma-Aldrich, USA) for 5 min, respectively. To preserve fluorescence, the film samples were protected with Fluoromount mounting medium (Sigma-Aldrich, USA). The quantitative analysis was performed by cell counting of the DAPI nuclei of 10 random fields with an area of 90,000 μ^2 to represent the entire film surface per group. These results were normalized to the total counted area in three independent experiments. The total number of DAPI-marked cells counted on the film surfaces was expressed as percentage with respect to the number of DAPI-marked cells counted on the surface of the glass coverslips (considered 100 %).

2.4.2. Antiviral test

The enveloped bacteriophage phi 6 (DSM 21518), which infects *Pseudomonas psyringae* (DSM 21482), both purchased from the Leibniz Institute DSMZ-German Collection of Microorganisms and Cell Cultures GmbH (Braunschweig, Germany), was used as surrogate for the enveloped SARS-CoV-2 for biosafety reasons [43–47]. Bacterial culture was first performed in solid tryptic soy agar (TSA, Liofilchem) and then in liquid tryptic soy broth (TSB, Liofilchem) at 120 r.p.m. and at 25 °C in a refrigerated incubator. Bacteriophage phi 6 propagation was performed according to the specifications provided by the Leibniz Institute DSMZ-German Collection of Microorganisms and Cell Cultures GmbH. Thus, 50 μL of bacteriophage suspension was added in TSB to each film disc at a titer of about 1×10^6 plaque-forming units per mL (PFU/mL) to be incubated for 24 h. Falcon tubes were prepared containing individual film discs with 10 mL of TSB sonicated for 5 min (at 25 °C), followed by 1-min of vortexing. Serial dilutions were performed subsequently from each falcon tube for bacteriophage titration. 100 μL of bacteriophage dilution was mixed with 100 μL of the host strain at an optical density (OD) of 0.5 at 600 nm. The double-layer assay was used to study the

infective capacity of the bacteriophage [48]. 4 mL of top agar (composed of TSB and 0.75 % bacteriological agar) from Scharlau (Ferrosa, Barcelona, Spain), 1 mM $CaCl_2$ and the infectious suspension (bacteriophage/bacteria) were mixed and poured onto TSA plates to be placed in a refrigerated incubator at 25 °C for 24 h. The antiviral capacity of the material films was determined at 24 h of viral contact, calculating the bacteriophage titers in log(PFU/mL) for comparative analysis with respect to the control: 50 μL of bacteriophage suspension was mixed with the bacteria without having been in contact with any material film disc. To avoid false results, it was checked that the sonication/vortexing processes had no effect on the infectious capacity of the bacteriophage and that the residual amounts of material films did not interfere with the titration procedure. Antiviral tests were performed in triplicate on two different days ($n = 6$) to provide reproducible results.

2.4.3. Double-stranded RNA extraction and quantification

Bacteriophage phi 6 RNA extraction and quantification were performed before and after being in contact with the material films to ensure that the viral particles did not remain adhered to the material films in the antiviral tests, which would have provided false antiviral results. These quantitative assays are important to make sure that the bacteriophages inactivate after being in contact with the material films. 50 μL of 1×10^6 PFU/mL bacteriophage concentration was placed on the material film discs and left to incubate at 25 °C for 24 h. 50 μL of the same bacteriophage dispersion was left to incubate at 25 °C for 24 h without having been in contact with the films (control). Subsequently, 10 mL of TSB were mixed with the samples to sonicate for 5 min and vortex for 45 s. RNA extraction was carried out immediately after vortexing, following the Canadian Norgen Biotek Corp's RNA extraction protocol [49]. A transparent mixture was produced by viral particle-lysing followed by RNA purification via binding to the purification column, washing the purification column and elution of the RNA for storage at −70 °C to prevent degradation. The amount of RNA in ng/μL was quantified in triplicate using a nanodrop spectrophotometer (Thermo Scientific, USA).

2.5. Physical and chemical characterization

2.5.1. Morphology

The addition of GNPs to the sample films produced a marked change of transparency. The opacity (O) of the sample films was calculated by Eq. (1) [40,50]:

$$O = \frac{Abs600}{x} \tag{1}$$

where Abs600 refers to the absorbance measured at a wavelength of 600 nm and x is the film thickness of the polymer mixture in mm.

An empty spectrophotometry cuvette, without any sample, was used as reference. The sample films were cut into a 4 mm × 50 mm rectangle and placed in a spectrophotometry cuvette to measure the absorbance in a spectrophotometer at a wavelength of 600 nm. Four replicates ($n = 4$) of each sample film were measured to ensure reproducibility.

The morphology of the sample films was studied by High-Resolution Field-emission Scanning Electron Microscopy (HR-FESEM) (GeminiSEM 500, Zeiss-Oxford Instruments) with an accelerating voltage of 1.5 kV. The cross-section was observed by cryogenic fracture with liquid nitrogen.

2.5.2. Water sorption

The water absorption capacity of the material films was studied at physiological temperature (37 °C). Sample films were cut into discs of equal diameter (10 mm) in dry state. After measuring their weight, they were placed in stoppered plastic vials filled with distilled water in a thermostatic bath at 37 °C and weighed at different time intervals (24, 48 and 120 h) after removing the residual water on the surface of the material by filter paper. The equilibrium water content (w_{eq}) of each material film, defined according to Eq. (2) [51] was then determined.

$$w_{eq} = \frac{(m_t - m_0)}{m_0} \tag{2}$$

where m_o is the mass of the material film disc in the dry state and m_t is the mass of the material film disc swollen in distilled water for a specific time.

Six replicates ($n = 6$) of each material were analysed under the same conditions to ensure the reproducibility of the method. The water absorption experiment is based mainly on the fact that the absorbed water content increases until reaching equilibrium, after which no further appreciable amount of water is absorbed.

2.5.3. Fourier transformed infrared spectroscopy

Functional groups were identified by Fourier transformed infrared spectroscopy (FTIR) on a Bruker Optics FTIR Alpha II at room temperature. FTIR spectra were collected in transmittance mode from 4000 to 300 cm^{-1} after 24 scans at a resolution of 2 cm^{-1}.

2.5.4. Thermogravimetric analysis

Measurements were performed by Thermogravimetric analysis (TGA) on a Mettler Toledo TGA 2 (small furnace system). Vacuum-dried samples (5–10 mg weight) were placed on the balance and the temperature raised from 25 to 700 °C at a rate of 10 °C/min. The mass of the sample was monitored as a function of temperature.

2.5.5. Differential scanning calorimetry

Differential scanning calorimetry (DSC) analysis was carried out on a PerkinElmer DSC 8000 under a flowing nitrogen atmosphere. The samples (5 to 10 mg) were vacuum-dried until constant weight to remove moisture and subjected to a cooling scan down to −15 °C, followed by a heating scan up to 250 °C at a rate of 20 °C/min.

2.5.6. Electrical conductivity

The electrical conductivity of the sample films was studied by a T2001A3-EU four-point probe machine (Ossila Limited, Sheffield, UK) using the following expression (4):

$$\sigma = \frac{1}{R_s \cdot l} \tag{4}$$

where R_s is the sheet resistance of a square sample (20 × 20 mm) and l is the sample thickness (≈100 μm). The measurements were performed in triplicate to ensure reproducibility.

2.6. Statistical analysis

All the statistical results and graphs were generated by ANOVA after Tukey's multiple post-hoc, applying GraphPad Prism 6 software. $p < 0.05$ were considered statistically significant.

3. Results and discussion

3.1. Synthesis

SA, a hydrophilic polymer, was mixed with the hydrophobic polymer PHBV in several ratios (10/90, 30/70 and 50/50 mixtures). The optimal PHBV/SA ratio was determined to be 10/90, which produced the most homogeneous mixture (Fig. 1). This composition is also the most economical, since the microbial polymer PHBV is much more expensive than sodium alginate. The SA chains in the mixture were subsequently crosslinked with Ca ions to form a semi-IPN (PHBV/CA 10/90 sample), preventing the dissolution of the sample in aqueous environments. The properties of pure SA or PHBV were improved in the PHBV/CA 10/90 semi-IPN. The schematic representation of the synthesis process and the

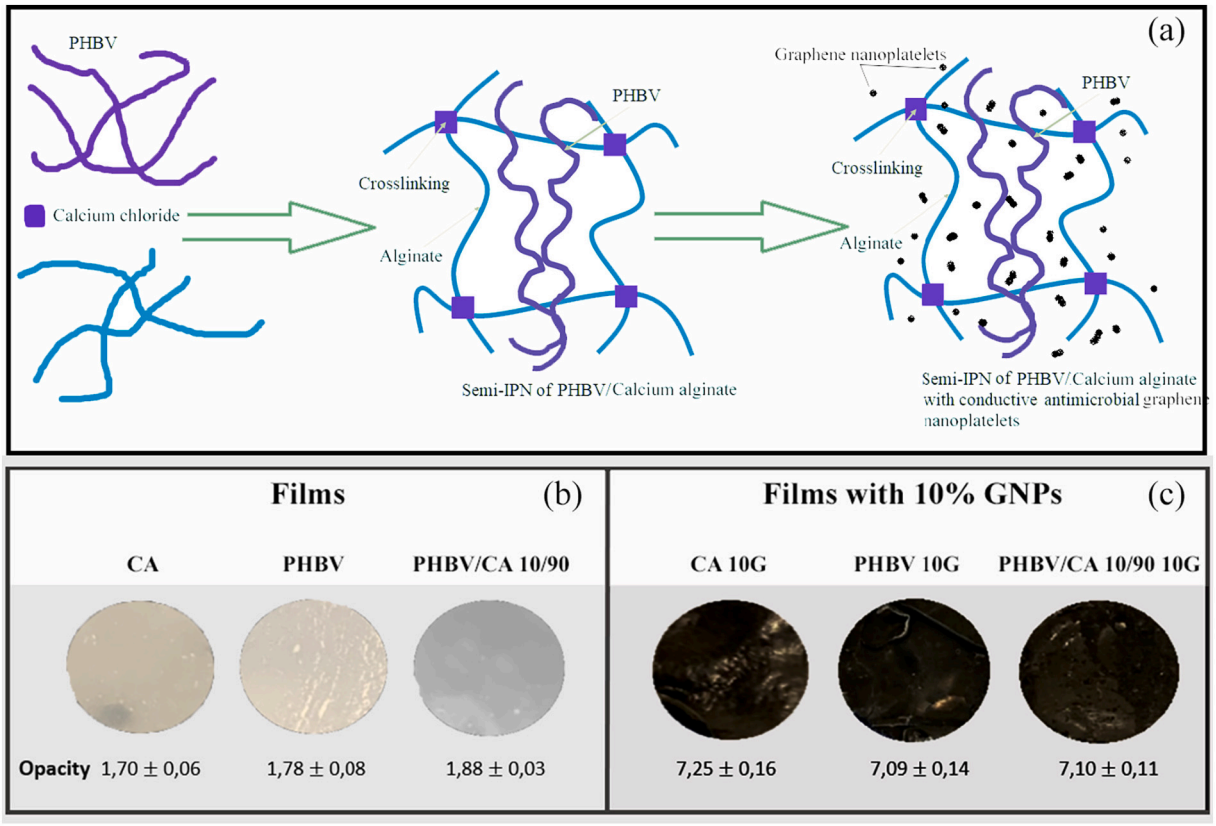

Fig. 2. Schematic representation of the synthesis process (a) and the macroscopic morphology of the novel biodegradable semi-interpenetrated polymer network (semi-IPN) of poly(3-hydroxybutyrate-*co*-3-valerate) and crosslinked alginate (with calcium chloride) without (b) and with (c) conductive antimicrobial graphene nanoplatelets; 10G: 10 % graphene nanoplatelets. The opacity of each film calculated by Eq. (1) is shown under each sample.

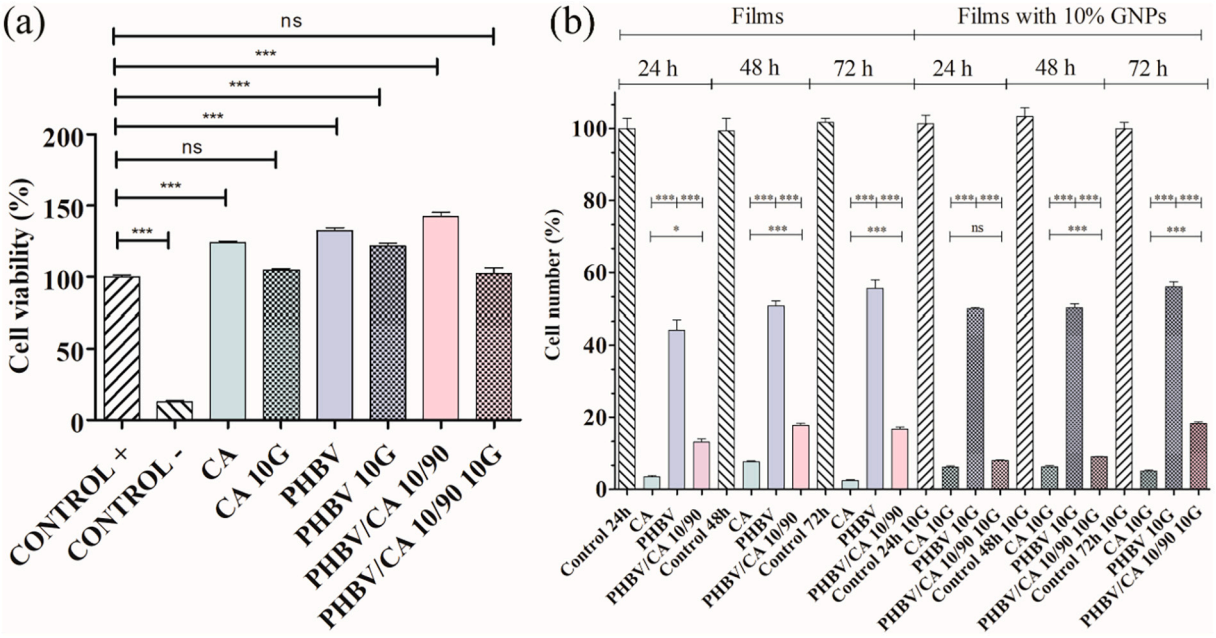

Fig. 3. Cell viability and quantitative cell adhesion: (a) cell viability in percentage of human keratinocyte HaCaT cells studied in the material film extracts according to ISO 10993-5:2009.; CONTROL +: the medium used to obtain the film extracts; CONTROL -: toxic zinc chloride solution. Data expressed as mean ± SD. *** $p <$ 0,001; ns: not significant.; (b) Quantitative analysis of cells on the surface of the films of CA, PHBV and semi-IPN PHBV/CA with and without 10 % *w*/w of GNPs after 24, 48 and 72 h h of incubation time. Cell count of the DAPI nuclei of 10 random fields with an area of 90,000 μ^2 to represent the entire film surface per group. Cell number expressed as percentage with respect to the total number of cells adhered to a glass cover slip (control) counted. Analysis performed with human keratinocyte HaCaT cells. CA: Calcium alginate, PHBV: Poly (3-hydroxybutirate-*co*-3-hydroxyvalerate); 10G: 10 % graphene nanoplatelets. Data expressed as mean ± SD. *** $p <$ 0,001; * $p <$ 0,05; ns: not significant.

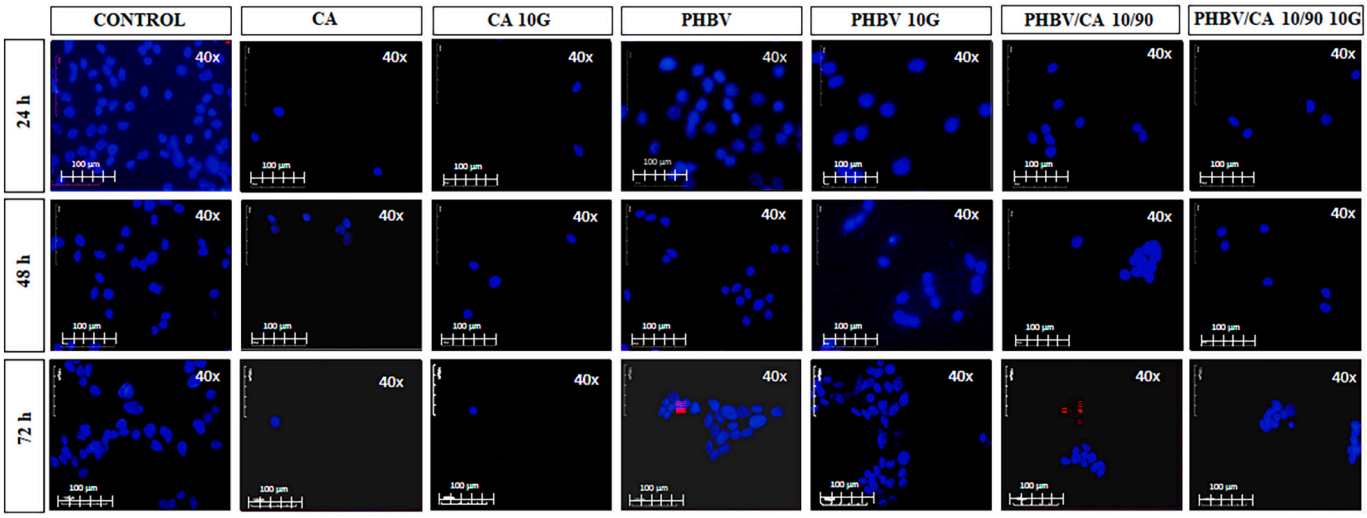

Fig. 4. Qualitative analysis of DAPI-marked cells counted on the biomaterial film surfaces of CA, PHBV and semi-IPN PHBV/CA with and without 10 % w/w of GNPs after 24, 48 and 72 h h of incubation time. Analysis performed with human keratinocyte HaCaT cells. Glass cover slip used as control. CA: Calcium alginate, PHBV: Poly (3-hydroxybutirate-*co*-3-hydroxyvalerate); 10G: 10 % graphene nanoplatelets.

structure of the biodegradable polymeric films are shown in Fig. 2a.

The physical appearance of the films of calcium alginate, PHBV and the semi-IPN of PHBV/CA with the optimal composition (10/90 *w/w*) with and without 10 % of GNPs are shown in Fig. 2b and c, respectively.

As expected, the addition of 10 % of GNPs clearly increases the opacity of the films (see opacity values determined by Eq. (1) in Fig. 2b and c). Graphene is a promising transparent conductor [52], however, the transparency of graphene materials decreases dramatically when the number of graphene layers is increased [53]. The opacity of the composites produced with these materials thus increases as a function of their graphene nanoplatelet content [54]. Similar increases in opacity have been reported with other CA composites containing even lower amounts of CNMs, such as graphene oxide (GO) [40,59] or carbon nanofibers (CNFs) [4]. The addition of CNFs or GO to PHBV also produces dark composite materials [15,60].

As far as we know, previous reports in the literature have not shown the development of biomaterial films based on PHBV and SA or CA. The latest related developments in this field consist of the production of alginic acid treated flax fibres/PHBV green composites in compost medium [55], microencapsulation of rifampicin in materials in alginate and in PHBV [56] and the enhancement of PHBV with Fingolimod by applying modified alginate [57]. The crosslinking of SA with divalent cations improves the tensile strength of SA [58], and gives this polymer the ability to absorb large amounts of water without being dissolved. The addition of carbon nanomaterials (CNMs) improves the mechanical properties of calcium alginate [4,59].

3.2. Characterization

3.2.1. Biological characterization

3.2.1.1. Cytotoxicity and cell adhesion. The MTT test was performed to study cytotoxicity using extracts of the prepared films in human HaCaT keratinocyte cells (Fig. 3a).

Fig. 3a clearly shows that none of the material films are cytotoxic and that the cell viability in some material films is even higher than the positive control. The semi-IPN network of PHBV/CA 10/90 thus showed good biocompatibility and null cytotoxicity, in good agreement with the literature, since PHBV and CA are fully biocompatible materials [11,14]. The addition of a large amount of conductive GNPs (10 % *w/w*) to the CA, PHBV and semi-IPN PHBV/CA does not produce any toxic effect in human keratinocytes.

After determining the null cytotoxicity of the material films, a cell adhesion study was performed on the surface. Qualitative and quantitative analyses were carried out to determine the cell adhesion properties based on the DAPI-marked cells counted on the biomaterial film surfaces. The results of the qualitative analysis of cell adhesion after culture for 24, 48 and 72 h are shown in Fig. 4. The quantitative analysis performed by cell counting the DAPI nuclei of 10 random fields with an area of 90,000 μ^2 to represent the entire film surface per group is shown in Fig. 3b.

Fig. 4 shows how the number of cells adhering to CA decreases dramatically with respect to control, since calcium alginate is a biomaterial with very low cell adhesion properties as has already been reported in the literature [33], although PHBV has even better cell adhesion properties than CA [60]. In good agreement with the previous results, it can be seen in Fig. 4 that more HaCaT cells adhered to the PHBV substrates than to CA after 24, 48 or 72 h. In addition, the small amount of PHBV incorporated into the CA polymer network improves CA cell adhesion (for example, the number of cells adhering to PHBV/CA 10/90 increases with respect to those adhering to CA after 24, 48 and 72 h), which shows it to be an alternative method of increasing cell adhesion in this hydrophilic biopolymer. However, adding GNPs hardly affects cell adhesion. In this regard, previous studies have shown that adding CNMs to CA [9] did not improve cell adhesion, in agreement with the present study. On the other hand, Rivera-Briso et al. showed that adding a much lower amount (1 % *w/w*) of CNMs to PHBV did enhance cell adhesion [60]. However, increasing the amount of CNMs (10 times higher than the present study) added to PHBV can significantly increase the chances of having large aggregates of carbon nanoparticles, which could worsen the cell adhesion properties. The presence of non-adherent CA in the semi-IPN of PHBV/CA 10/90 10G could also worsen the cell adhesion properties and somehow explain these results.

GNPs have shown to be promising nanomaterials capable of up-regulating specific genes involved with many important features required in biomedical fields such as wound healing and skin tissue engineering [39].

3.2.1.2. Antiviral activity. The phi 6 bacteriophage, a double-stranded RNA virus with a non-linear fragmented length of 13.5 kb belonging to the Baltimore Group III [61], was used as viral model for SARS-CoV-2 for biosafety reasons [44,46,62]. This bacteriophage is also used as biosafe viral model of other enveloped viruses such as Ebola and Influenza. The results of the antiviral tests are shown in Fig. 5. Cross-linked

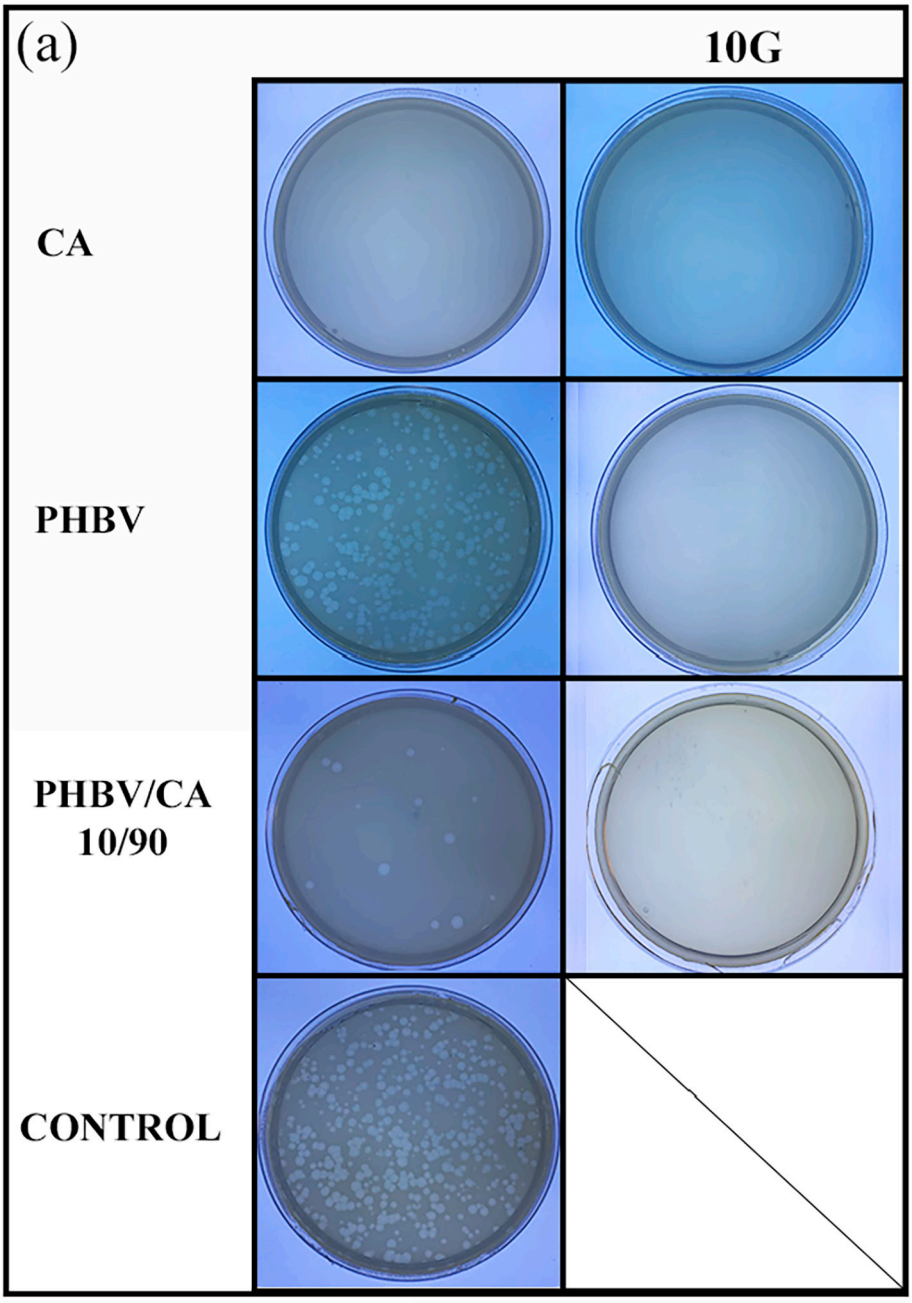

(b) Sample	Bacteriophage Phi 6 at 24 h (PFU/mL)
CONTROL	$6.42 \times 10^6 \pm 3.22 \times 10^5$
CA	0.0 ± 0.0
CA 10G	0.0 ± 0.0
PHBV	$4.48 \times 10^6 \pm 2.69 \times 10^5$
PHBV 10G	0.0 ± 0.0
PHBV/CA 10/90	$3.00 \times 10^5 \pm 1.10 \times 10^5$
PHBV/CA 10/90 10G	0.0 ± 0.0

Fig. 5. Antiviral results: a) Loss of viability of bacteriophage phi 6 calculated from the double-layer essay, where the images refer to the titration of the phage for the control, PHBV, CA and semi-IPN PHBV/CA with and without the addition of 10 % GNPs at 24 h of viral contact, and b) Reduction of the infection titers of the samples. Data expressed as mean ± SD. *** $p < 0,05$; ns: not significant. CA: Calcium alginate, PHBV: Poly (3-hydroxybutirate-*co*-3-hydroxyvalerate); 10G: 10 % graphene nanoplatelets.

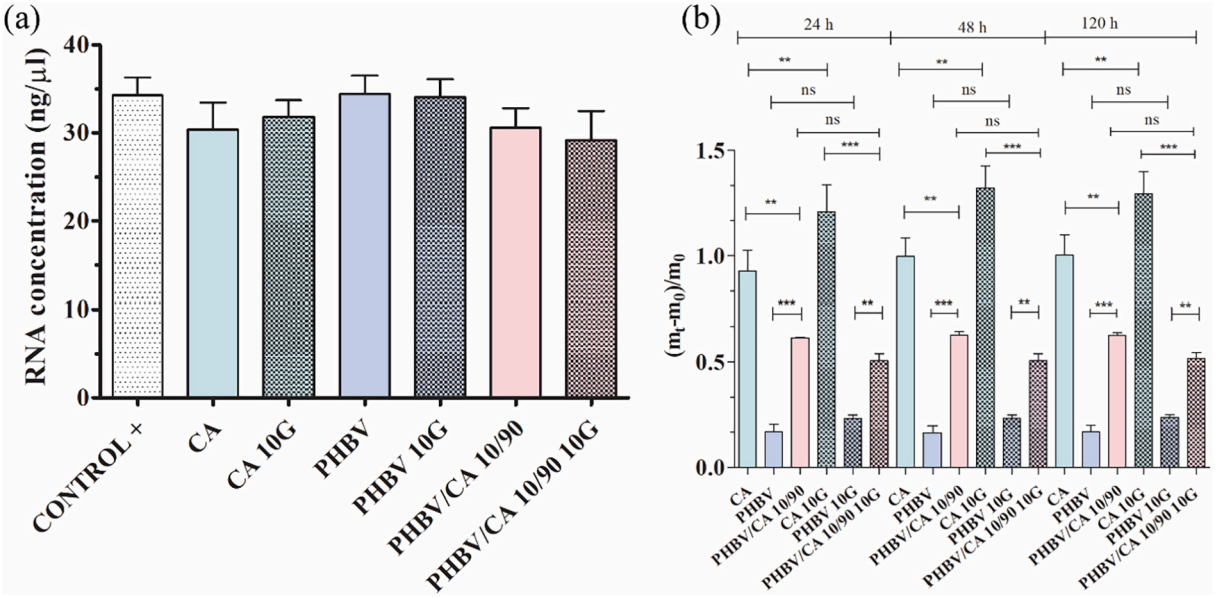

Fig. 6. *RNA concentration analysis and water sorption properties: (a) v*iral presence before (CONTROL +) and after the antiviral assay by extraction, purification, and quantification of phage phi 6 dsRNA to ensure no viral adhesion to the material films during the antiviral tests. ANOVA after Tukey's multiple post-hoc applying GraphPad Prism 6 software with a significance of at least $p < 0.05$. The results of the statistical analysis showed no statistical differences between the samples.*; (b) w*ater sorption at body temperature (37 °C ± 0,5 °C) at 24, 48 and 120 h of water immersion times. The amount of absorbed water is expressed as $(m_t\text{-}m_0)/m_0$ for each material film, where m_t is the mass of the sample film at time t and m_0 is the initial mass of the dry sample film. Data were expressed as mean ± SD. *** p < 0,05; ns: not significant. CA: Calcium alginate, PHBV: Poly (3-hydroxybutirate-*co*-3-hydroxyvalerate), 10G: 10 % graphene nanoplatelets. ANOVA after Tukey's multiple post-hoc. Data expressed as mean ± SD. *** $p < 0,001$; ** $p < 0,01$; ns: not significant.

alginate shows 100 % of antiviral activity against bacteriophage phi 6, as no plaque forming units (PFU) appear on the plaque when compared to the control sample formed by bacteriophages that had not been previously in contact with any material. Neat PHBV shows no antiviral activity, similar to control. However, when CA is combined with PHBV in the semi-IPN, a >1 log reduction of PFU/mL takes place. When 10 % GNPs are added to CA, PHBV or PHBV/CA 10/90 films, there is 100 % of antiviral activity.

These results are in agreement with previous findings obtained using calcium alginate against another enveloped virus such as SARS-CoV-2 Delta variant [6,7]. The antiviral mechanism of calcium alginate is not yet clear, but it can be attributed to the charged polymer network that can bind to viral envelopes, inactivating its replication. As far as we know, the null antiviral activity of PHBV has been demonstrated here for the first time. We also provide a successful method of producing composite PHBV materials with antiviral properties. CBNs are well-known to possess broad spectrum antimicrobial properties [8,16], however, their antimicrobial activity after incorporation into polymer matrices depends on the amount of CBNs added [12,63]. Polymers can act like plastic bags covering antimicrobial nanomaterials, thus reducing their antimicrobial potential.

In order to ensure that the antiviral results are correct and no viral particles remain in the material films during the antiviral tests, viral RNA was extracted and measured. This experiment was performed before and after the viral particles had been in contact with the material surfaces to be compared for 24 h. Fig. 6a shows that the samples have a dsRNA concentration similar to that of the positive control, and that in all cases the CA and semi-IPN PHBV/CA 10/90 samples with and without 10 % graphene have lower values than the PHBV sample.

The potent antiviral activity of CA and GNPs in the PHBV/CA 10/90 10G semi-IPN can be attributed to their compacted negative charges produced during the solvent casting process. The negatively charged CA polymer chains [7] and GNP nanosheets [8] may therefore bind to viral envelopes, inactivating membrane receptors. The amount of GNPs (10 % *w*/w) was determined experimentally to provide the semi-IPN films with significant conductive properties. In agreement with these results, adding another type of CNMs to CA, particularly CNFs, enhanced CA antiviral activity [10].

3.2.2. *Physical characterization techniques*

3.2.2.1. Morphology. The cryogenic fractures of the films observed by HR-FESEM are shown in Fig. 7.

The GNPs can be appreciated in the CA and PHBV composites (see yellow arrows for CA 10G and PHBV 10G in Fig. 7). The semi-IPN structure of PHBV/CA 10/90 clearly shows a biphasic structure by HR-FESEM, with PHBV microdomains in a darker tone than CA. However, these heterogeneous structure changes dramatically when 10 % of GNPs is added.

In the semi-IPN of PHBV/CA, a clear phase separation can be seen with microdomains of darker PHBV (see red arrows for PHBV/CA 10/90 in Fig. 7). The semi-IPN with 10 % of GNPs (PHBV/CA 10G) shows some alignment of the GNP nanosheets (see yellow arrows in Fig. 7). However, the HR-FESEM micrographs of the CA 10G and PHBV 10G composite films show irregular morphologies with aggregates of GNPs. This might explain why the incorporation of this large amount of aggregated GNPs (10 % *w/w*) did not improve cell adhesion (Fig. 3b and 4).

3.2.2.2. Water sorption. Water sorption experiments performed at 37 °C show the equilibrium water content determined by Eq. (2) at different time intervals: 24, 48 and 120 h (Fig. 6b).

While CA is a highly hydrophilic material, PHBV is highly hydrophobic, so that the former presents much higher equilibrium water sorption values than the latter. The semi-IPN PHBV/CA 10/90 presents an intermediate value with statistically significant differences between the three materials. The water sorption equilibrium is seen to be reached after 24 h because the water sorption values at 24, 48 and 72 h are similar for each sample film. The addition of 10 % GNPs slightly increased the water sorption of the neat CA hydrogels. This slight increase in water sorption at 37 °C can be attributed to the fact that GNPs are hydrophobic [64] but produce graphitic nanochannels in the CA

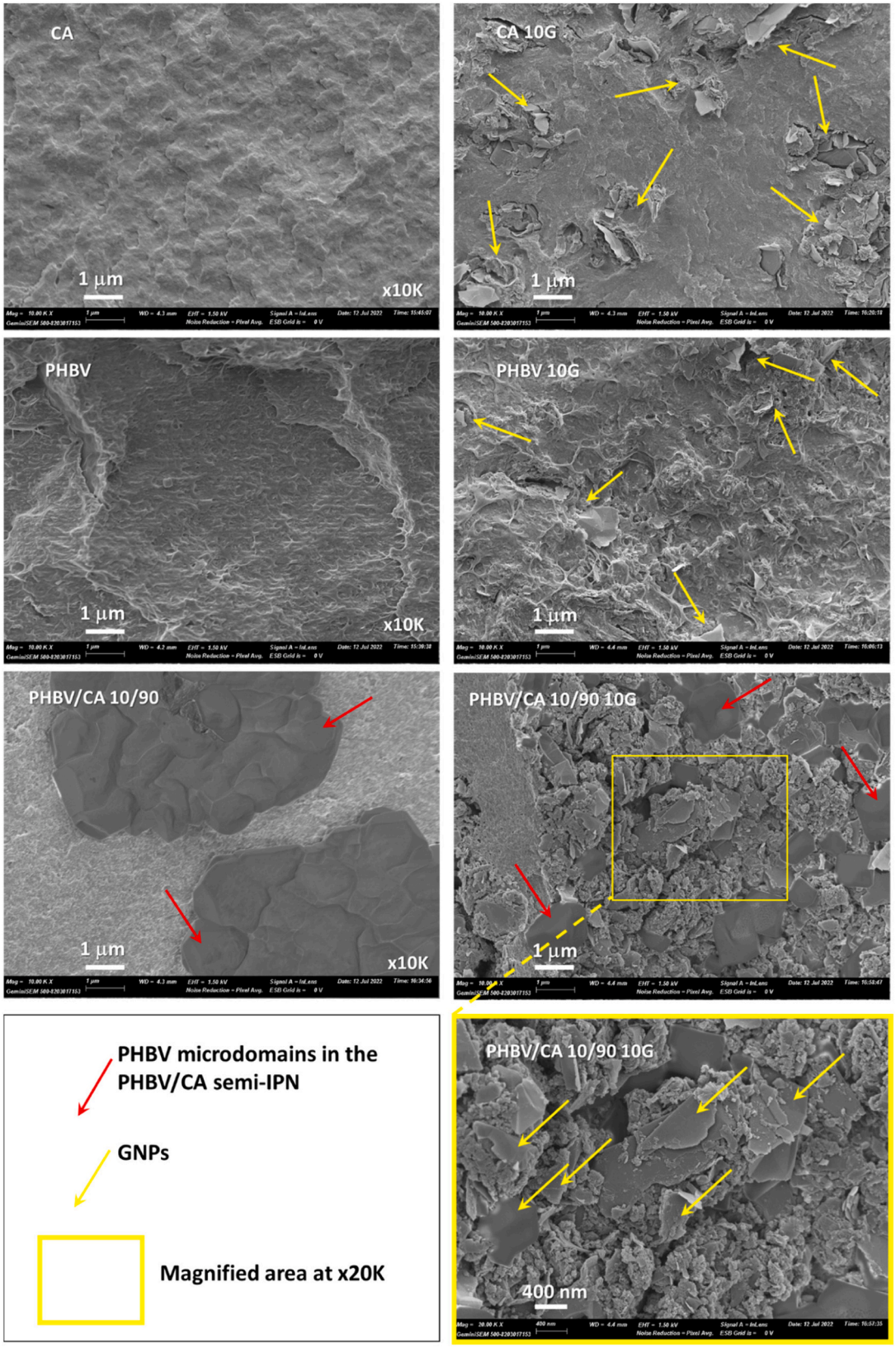

Fig. 7. Material morphology: HR-FESEM observation after cryogenic fracture of the calcium alginate (CA), PHBV and semi-IPN PHBV/CA 10/90 sample films with and without 10 % of GNPs (10 G) at x10000 and a magnified area at x20000. Yellow and red arrows indicate the GNPs present in the nanocomposites and microdomains of PHBV in the semi-IPN of the PHVA/CA 10/90 with and without 10 % of GNPs, respectively. (For interpretation of the references to colour in this figure legend, the reader is referred to the web version of this article.)

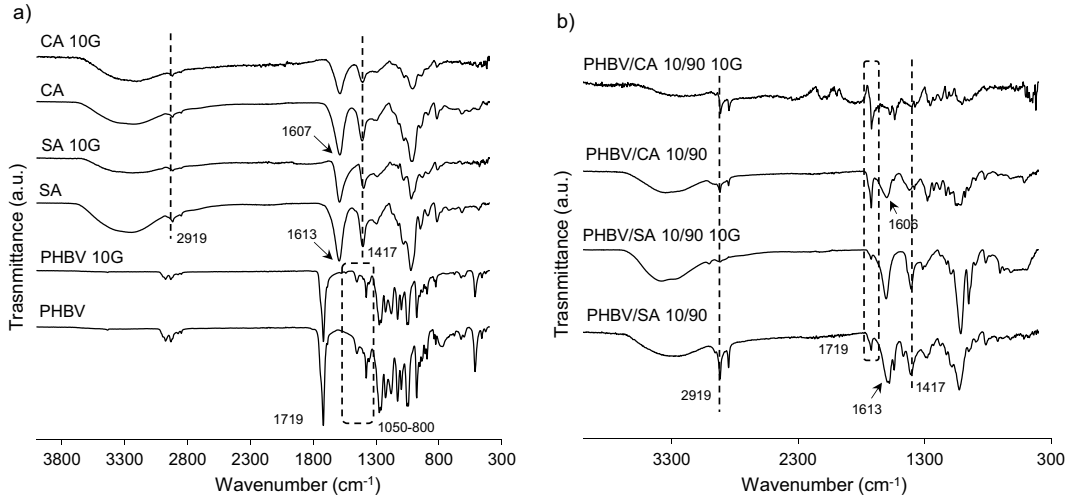

Fig. 8. Fourier transform infrared spectroscopy (FTIR) spectra in the region 4000–300 cm^{-1}. a) Neat PHBV, SA and calcium alginate (CA), and samples with 10 % of graphene nanoplatelets (10 G). b) PHBV/SA 10/90 blend, semi-IPN PHBV/CA 10/90, and nanocomposites with GNPs (10G). GNPs concentration: 10 % *w/w*.

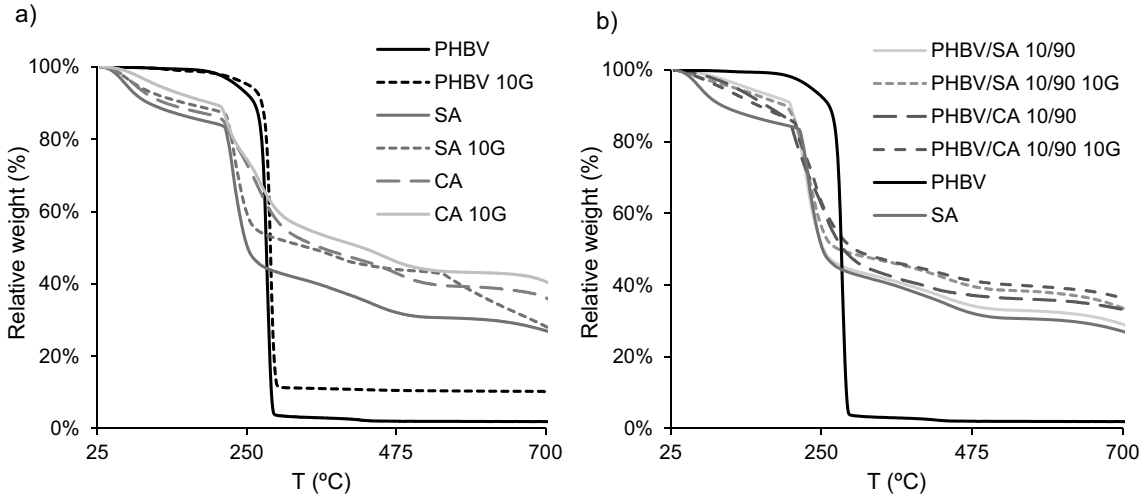

Fig. 9. Thermogravimetry results. (a) Neat SA and PHBV and crosslinked CA with and without 10 % of graphene nanoplatelets (10 G). (b) PHBV/SA 10/90 blend, semi-IPN PHBV/CA 10/90 and nanocomposites with GNPs (10G). GNPs concentration: 10 % *w/w*. Neat SA, CA and PHBV have also been included in b) as reference samples.

polymer network that make water molecule penetration easier [65]. However, no significant statistical effect was found on water sorption after adding GNPs to the PHBV or PHBV/CA 10/90 films.

3.2.2.3. Fourier transform-infrared spectroscopy. Fig. 8 shows the FTIR spectra of the samples. PHBV, SA and CA with and without GNP have been included as reference in Fig. 8a.

The neat PHBV spectrum shows a band at 1719 cm^{-1} related to the C═O stretch of the ester group present in the molecular chain of the highly ordered crystalline structure. The peaks between 800 and 1050 cm^{-1} are characteristic of the -C–O–C- stretching vibration [2,66,67] (Fig. 8a). Regarding neat SA, the wide band between 3700 and 3000 cm^{-1} is associated with O—H stretching and the peaks at 2919 cm^{-1} and 1417 $cm^{-1}$are related to C—H stretch sp^3 and C-OH stretch, respectively [68,69]. Crosslinking SA with $CaCl_2$ replaces sodium with calcium ions, a reaction that produces a change in ion density, diameter and weight, affecting the applied stretch forces to the C═O carboxylic salt functional groups [70], so that a slight shift can be seen from 1614 cm^{-1} in neat SA to 1606 cm^{-1} in CA (Fig. 10a) [68].

The spectrum of the PHBV/SA blend, depicted in Fig. 8b, shows the characteristic peaks related to both PHBV and SA, confirming their presence in the blend. Likewise, the semi-IPN PHBV/CA obtained after crosslinking the SA chains with Ca^{+2} ions also shows the slight shift corresponding to the stretch in the C═O carboxylic salt functional groups (from 1613 to 1606 cm^{-1}).

As pristine graphene does not show any significant peaks related to

Table 3
50 % weight loss decomposition temperature for the different samples.

Sample	$T_{d\text{-}50\%}$ (°C)
PHBV	278
PHBV 10G	285
SA	250
SA 10G	344
CA	362
CA 10G	423
PHBV/SA 10/90	253
PHBV/SA 10/90 10G	275
PHBV/CA 10/90	282
PHBV/CA 10/90 10G	299

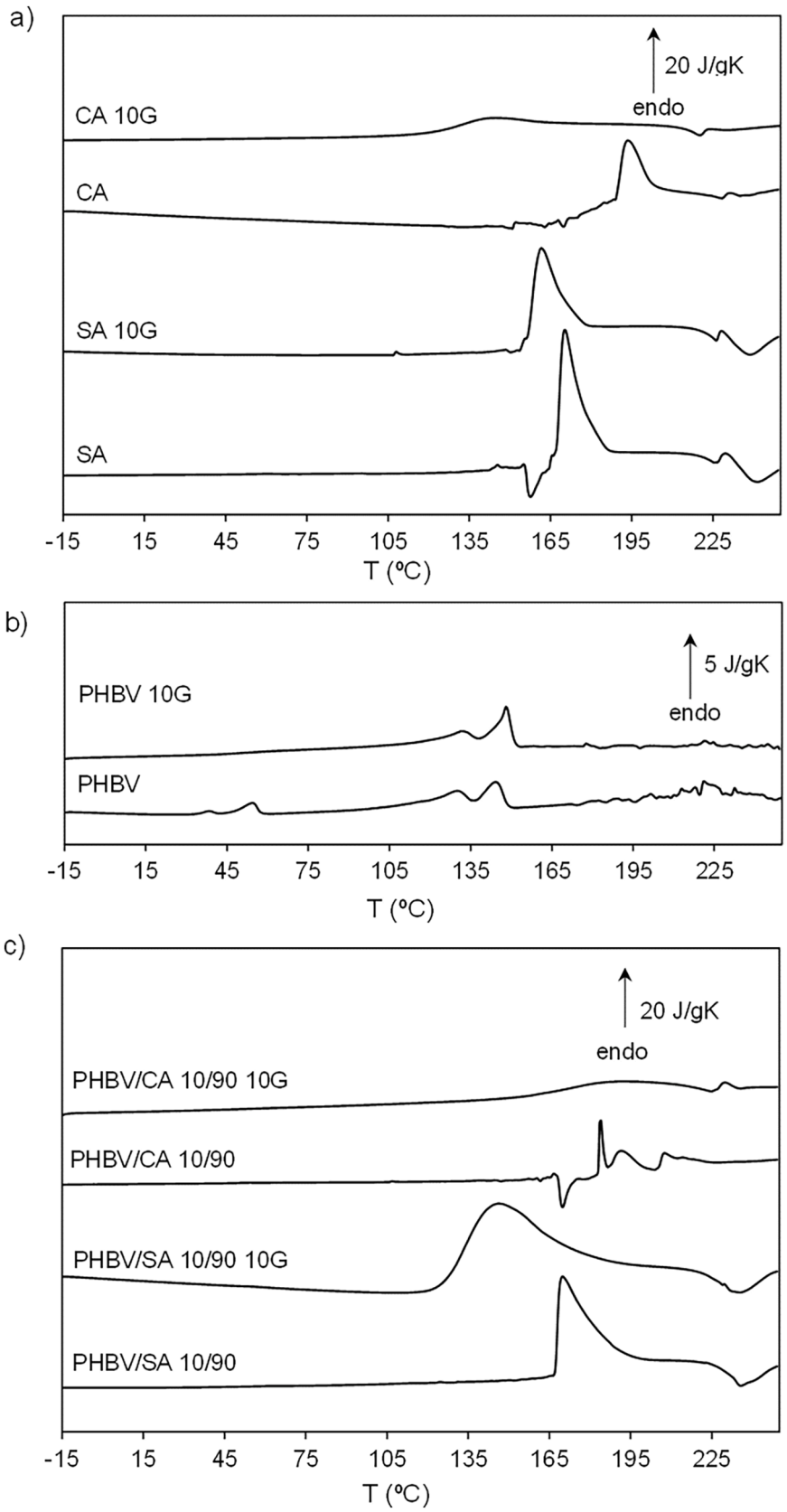

Fig. 10. Differential scanning calorimetry (DSC) thermograms at a rate of 20 °C/min Normalized heat flow on heating. (a) Neat SA and crosslinked SA (CA) with and without GNPs (10 G). (b) Neat PHBV with and without GNPs (10 G). (c) PHBV/SA 10/90 blend, PHBV/CA 10/90 semi-IPN and nanocomposites with GNPs (10G). GNPs concentration: 10 %.

functional groups [71,72], incorporating graphene is not seen in the FTIR spectra.

3.2.2.4. Thermal degradation analysis. Thermal degradation was analysed by TGA. Fig. 9 shows the thermogravimetry results from 25 to 700 °C. The decomposition temperatures at 50 % weight loss ($T_{d\text{-}50\%}$), which are representative of the thermal decomposition behaviour of this system, were subsequently calculated from the TGA profiles (Table 3).

Neat PHBV (Fig. 9a) shows a single degradation stage, which begins at 225 °C. $T_{d\text{-}50\%}$ is 278 °C, and at 300 °C the polymer is almost completely degraded due to hydrolysis and chain scission [2,73,74]. SA shows an initial weight loss related to moisture removal, i.e. free and bound water molecules, at temperatures lower than 225 °C. The interval between 225 and 275 °C corresponds to the maximal thermal decomposition, followed by a second process in the 275–500 °C range. These degradation stages are related to the SA matrix degradation, followed by the formation of metal carbonates at higher temperature [70,75]. The degradation continues above 500 °C. SA crosslinking increases thermal stability ($T_{d\text{-}50\%}$ increases from 250 °C for neat SA to 344 °C for crosslinked CA). PHBV/SA blend and semi-IPN PHBV/CA thermal degradation profiles are depicted in Fig. 9b. Neat SA and PHBV have also been included to facilitate understanding the results. As can be observed, the degradation profile follows SA behaviour, the main component of the blend. The presence of 10 % of the hydrophobic PHBV reduces the amount of water molecules bounded to the SA chains, leading to lower weight loss than SA during the first degradation process below 225 °C, both in the blend and semi-IPN. The crosslinking of the SA chains in the mixture, forming the semi-IPN, increases thermal stability. The 50 % weight loss decomposition temperature, $T_{d\text{-}50\%}$, increases from 253 °C for the PHBV/SA blend to 282 °C in the semi-IPN PHBV/CA.

Adding 10 % of GNPs affects the degradation profile of PHBV, SA and CA, increasing their thermal stability. After adding GNPs, $T_{d\text{-}50\%}$ of PHBV 10G rises ca. 7 °C compared to neat PHBV, whilst in SA 10G and CA 10G samples the increase is much higher (Table 3).

The thermal degradation profile of the PHBV/SA 10/90 blend and PHBV/CA 10/90 semi-IPN with and without GPNs is similar to SA/CA, which is consistent with 90 % of alginate in the total polymeric mass (Fig. 9b). As expected, SA crosslinking increases thermal stability in the semi-IPN compared to the PHBV/SA 10/90 blend [20]. The incorporation of 10 % GNPs affects the degradation profile in the PHBV/SA 10/90 blend and PHBV/CA 10/90 semi-IPN, increasing thermal stability ($T_{d\text{-}50\%}$ increases from 253 to 275 °C in the blend and from 282 to 299 °C in the semi-IPN). This noticeable rise can be attributed to obstacles to the diffusion of volatile decomposition products within the polymeric matrix (particularly, a jammed network of char layers) [72,76,77]. It has also been reported that decomposition of graphene nanocomposites is slower due to restricted mobility of the chains of the polymer matrix around the graphene nanoparticles [76]. It can therefore be concluded that thermal stability increases after adding both Ca^{2+} ions and GNPs.

3.2.2.5. Thermal behaviour (DSC). The normalized heat flow of SA and crosslinked SA (CA) with and without GNPs is depicted in Fig. 10a.

The endotherm peak at temperatures above 120 °C is related to release of water tightly bonded through polar interactions with carboxylate groups (although the samples were vacuum-dried at 60 °C) [78,79]. As expected, the intensity of this peak after crosslinking SA decreases, indicating the presence of bonds between Ca ions and carboxylate groups, which can no longer link to water molecules. In agreement with the TGA results, the beginning of the SA thermal degradation can be seen at 225 °C. As adding GNPs (10 %) increases hydrophobicity, the presence of water molecules bonded to the SA chains, particularly in the CA sample, is significantly reduced. Fig. 10b shows the heating scan of neat PHBV with and without GNPs. A small cold crystallisation process between 30 and 60 °C can be seen in the PHBV thermogram, followed by melting (120 and 150 °C) [2,80]. After graphene addition, there is no cold crystallisation process and only the peaks (of larger size) related to the melting process can be observed. The enthalpy of fusion increases from 26 J/g (PHBV) to 43 J/g (PHBV 10G), which indicates that GNPs act as nucleating agents for PHBV, increasing its crystallinity.

Table 2
Surface electric conductivity of neat PHBV, crosslinked SA and PHBV/SA 10/90 with and without 10 % GNPs.

Sample	σ(mS/m)
CA	1.4 ± 0.9
CA 10G	1.2 ± 0.1
PHBV	6.2 ± 1.8
PHBV 10G	6.8 ± 1.1
PHBV/CA 10/90	2.6 ± 1.5
PHBV/CA 10/90 10G	274.9 ± 7.7

The PHBV/SA blend heating scan with and without GNPs is depicted in Fig. 10c. The thermograms are similar to those of neat SA with and without GNPs. No melting process related to PHBV can be seen, although the amount of PHBV in the blend/semi IPN is low (10 %), which could prevent its visualisation. The peak associated with water bonded with SA chains can be seen in the blend with and without GNPs in the same temperature range as neat components (> 125 °C). The semi-IPN PHBV/CA thermogram shows a significant reduction in this process, which is further reduced after the addition of GNPs. The CA network hinders water molecules linked to the hydrophilic chains after the formation of the semi-IPN. Furthermore, due to the compact structure induced by crosslinking, the water molecules that remain strongly bound to the CA chains, also with PHBV chains entangled in the CA network, need more energy to be released, shifting the process towards a higher temperature (up to 210 °C). Adding GNPs increases the hydrophobic behaviour of the PHBV/CA 10/90 nanocomposite, reducing the peak related to the release of bound water, which is also an indicator of good graphene dispersion within the sample. The thermal degradation of the composites starts from 225 °C, in agreement with the TGA results (Fig. 8).

3.2.2.6. Electrical conductivity. The surface electrical conductivity is reported in Table 2 for the sample films: neat PHBV, crosslinked SA and the semi-IPN PHBV/SA 10/90, with and without 10 % GNPs. Neat CA and PHBV polymers have low conductivity values, although PHBV conductivity is slightly higher. The semi-IPN PHBV/CA shows a slight increase in surface conductivity consistent with the proportion of both components (10/90 ratio).

The addition of graphene to both PHBV and crosslinked SA hardly affects CA and PHBV film conductivity, with values in the range between 1 and 7 mS/m, which are quite low considering that the samples contain 10 % GNPs. However, adding GNPs to the PHBV/CA semi-IPN (PHBV/CA 10/90 10G sample) had a dramatic effect on electrical behaviour. Conductivity increased >40-fold (compared to PHBV 10G), reaching an average value ca. 275 mS/m.

The electrical conductivity of nanomaterials with conductive fillers is known to depend on filler type, shape, size and filler dispersion and distribution in the composite [81,82]. The processing method (e.g. melt blending or solution casting) also influences the final conductivity of the nanocomposite as well as the specific solvents used in the solution cast method and the drying rate used to evaporate the solvent [83,84]. The lower values of surface conductivity found for neat PHBV and CA nanocomposites after the addition of 10 % of GNP suggest a non-homogeneous distribution of the nanofiller in the polymer matrix, in agreement with the presence of GNP aggregates, as shown in the HR-FESEM images (Fig. 7). The PHBV/CA 10G nanocomposite was obtained by mixing three solvents (chloroform, DMSO and water), which can strongly influence viscosity and nanoparticle dispersion. The casting solvent has been identified as a key parameter that influences the

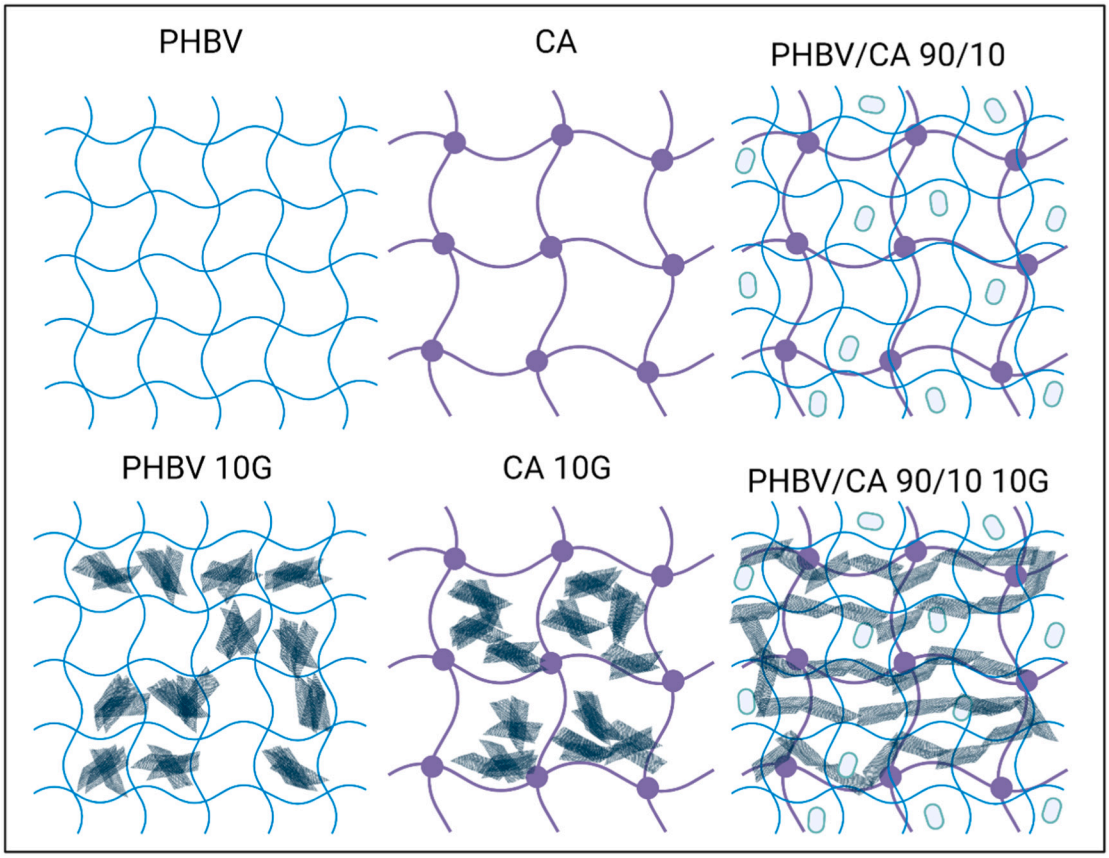

Fig. 11. Representative scheme of poly (3-hydroxybutirate-*co*-3-hydroxyvalerate) (PHBV:), calcium alginate (CA), semi-IPN PHBV/CA (PHBV/CA 10/90) with and without 10 % *w/w* graphene nanoplatelets (10 G). The conductive structure of the PHBV/CA 10/90 10G sample can be clearly seen by the continuity of the GNP sheets represented as a black trapezoid. The solid circle (●) represents the crosslinked points produced by divalent calcium cations. The blue ellipses represent the microdomains of PHBV present in the semi-IPNs PHBV/CA 10/90 and PHBV/CA 10/90 10G. Created with Biorender by Ángel Serrano-Aroca. (For interpretation of the references to colour in this figure legend, the reader is referred to the web version of this article.)

morphology and electrical properties of nanocomposites with conductive carbon nanoparticles [83,85,86]. The high value of surface conductivity obtained in the PHBV/CA 10/90 10G nanocomposite suggests that this specific combination of solvents facilitates the alignment of the GNPs within the complex polymer matrix formed by CA and PHBV, inducing the formation of effective electrical pathways and significantly increasing conductivity (Fig. 11). HR-FESEM images (Fig. 7) show well-distributed GNPs in the PHBV/CA 10/90 10G nanocomposite, consistent with increased conductive properties. CA 10G and PHBV 10G samples show the presence of multiple aggregates, which could explain the lower conductivity values. Further studies will be needed to analyse the role of this solvent mixture in the dispersion of the GNPs within the PHBV/CA matrix.

All these results confirm the novelty of these new advanced materials and show their great promise in the biomedical field.

4. Conclusions

A new biomaterial film based on PHBV and CA with potent antiviral activity, enhanced cell adhesion capacity and conductive properties was developed, containing 10 % *w/w* of GNPs in the form of semi-IPN. This new composite biomaterial showed enhanced physical and biological properties with respect to its neat components, CA and PHBV. Water sorption experiments at the physiological temperature (37 °C), FTIR analysis, thermal behaviour and degradation and electrical conductivity showed physical and chemical properties with great potential in the biomedical field, especially for antiviral technologies, electroactive sensors or regenerative medicine applications where electro-stimulation is required. This new biomaterial has also shown no cytotoxicity in human keratinocyte cells and improved biological properties, including cell adhesion (an essential issue for skin tissue engineering), and a strong antiviral activity with the incorporation of 10 % GNPs against a viral model of enveloped viruses such as SARS-CoV-2.

CRediT authorship contribution statement

A.H: Experiments, Data curation, Formal analysis, Writing – original draft; A.C-V., A. T-M, B.S: Experiments, Supervision; J.L.A-C: Experiments, Data curation, Formal analysis; R.S.i.S.: Conceptualization, Supervision, Investigation, Writing – original draft, Writing-reviewing and editing, Funding acquisition; A.S-A: Conceptualization, Supervision, Investigation, Writing – original draft, Writing-reviewing and editing, Funding acquisition.

Declaration of competing interest

The findings of this study contributed to patent application P202230138 to the OEPM Office, Madrid, Spain, with Á.S-A. and R.S.i.S as inventors. The remaining authors declare no competing interests.

Acknowledgments

This research was funded by the Fundación Universidad Católica de Valencia San Vicente Mártir, Grant 2020-231-006UCV, the Spanish Ministry of Science and Innovation (PID2020-119333RB-I00/AEI/10.13039/501100011033) (awarded to Á.S-A), and the FEDER/Spanish

Ministry of Science and Innovation-Agencia Estatal de Investigación through the Project RTI2018-097862-B-C21 (awarded to R.S.i.S). CIBER-BBN is an initiative funded by the VI National R&D&I Plan 2008–2011, Iniciativa Ingenio 2010, Consolider Program. CIBER Actions are financed by the Instituto de Salud Carlos III with assistance from the European Regional Development Fund.

References

[1] P. Ruano, L.L. Delgado, S. Picco, L. Villegas, F. Tonelli, M. Merlo, J. Rigau, D. Diaz, M. Masuelli, in: We Are IntechOpen, the World' s Leading Publisher of Open Access Books Built by Scientists, for Scientists TOP 1 %, Intech, 2016, p. 13, https://doi.org/10.5772/57353.

[2] J.L. Aparicio-Collado, J.J. Novoa, J. Molina-Mateo, C. Torregrosa-Cabanilles, Á. Serrano-Aroca, R. Sabater i Serra, Novel semi-interpenetrated polymer networks of poly(3-hydroxybutyrate-co-3-hydroxyvalerate)/poly (vinyl alcohol) with incorporated conductive polypyrrole nanoparticles, Polymers (Basel) 13 (2020) 57, https://doi.org/10.3390/polym13010057.

[3] N. Zoratto, P. Matricardi, Semi-IPNs and IPN-based hydrogels, in: I.B. Kunal Pal (Ed.), Polym. Gels, Elsevier Ltd, 2018, pp. 91–124, https://doi.org/10.1016/b978-0-08-102179-8.00004-1.

[4] M. Llorens-Gámez, B. Salesa, Á. Serrano-Aroca, Physical and biological properties of alginate/carbon nanofibers hydrogel films, Int. J. Biol. Macromol. 151 (2020) 499–507, https://doi.org/10.1016/j.ijbiomac.2020.02.213.

[5] Á. Rivera-Briso, A.L. Aachmann, F.L. Moreno-Manzano, V. Serrano-Aroca, Graphene oxide nanosheets versus carbon nanofibers: enhancement of physical and biological properties of poly (3-hydroxybutyrate-co-3-hydroxyvalerate) films for biomedical applications, Int. J. Biol. Macromol. 143 (2020) 1000–1008.

[6] Á. Serrano-Aroca, M. Ferrandis-Montesinos, R. Wang, Antiviral properties of alginate-based biomaterials: promising antiviral agents against SARS-CoV-2, ACS Appl. Bio Mater. 4 (2021) 5897–5907, https://doi.org/10.1021/acsabm.1c00523.

[7] A. Cano-Vicent, R. Hashimoto, K. Takayama, Á. Serrano-Aroca, Biocompatible films of calcium alginate inactivate enveloped viruses such as SARS-CoV-2, Polymers (Basel) 14 (2022) 1483, https://doi.org/10.3390/polym14071483.

[8] Á. Serrano-Aroca, K. Takayama, A. Tuñón-Molina, M. Seyran, S.S. Hassan, P. Pal Choudhury, V.N. Uversky, K. Lundstrom, P. Adadi, G. Palù, A.A.A. Aljabali, G. Chauhan, R. Kandimalla, M.M. Tambuwala, A. Lal, T.M. Abd El-Aziz, S. Sherchan, D. Barh, E.M. Redwan, N.G. Bazan, Y.K. Mishra, B.D. Uhal, A. Brufsky, Carbon-based nanomaterials: promising antiviral agents to combat COVID-19 in the microbial-resistant era, ACS Nano 15 (2021) 8069–8086, https://doi.org/10.1021/acsnano.1c00629.

[9] B. Salesa, M. Llorens-Gámez, Á. Serrano-Aroca, Study of 1D and 2D carbon nanomaterial in alginate films, Nanomaterials 10 (2020), https://doi.org/10.3390/nano10020206.

[10] I. Sanmartín-Santos, S. Gandía-Llop, B. Salesa, M. Martí, F. Lillelund Aachmann, Á. Serrano-Aroca, Enhancement of antimicrobial activity of alginate films with a low amount of carbon nanofibers (0.1% w/w), Appl. Sci. 11 (2021) 2311, https://doi.org/10.3390/app11052311.

[11] B. Salesa, M. Martí, B. Frígols, Á. Serrano-Aroca, Carbon nanofibers in pure form and in calcium alginate composites films: new cost-effective antibacterial biomaterials against the life-threatening multidrug-resistant Staphylococcus epidermidis, Polymers (Basel) 11 (2019) 453, https://doi.org/10.3390/polym11030453.

[12] M. Martí, B. Frígols, B. Salesa, Á. Serrano-Aroca, Calcium alginate/graphene oxide films: reinforced composites able to prevent Staphylococcus aureus and methicillin-resistant Staphylococcus epidermidis infections with no cytotoxicity for human keratinocyte HaCaT cells, Eur. Polym. J. 110 (2019) 14–21, https://doi.org/10.1016/J.EURPOLYMJ.2018.11.012.

[13] A.L. Rivera-Briso, F.L. Aachmann, V. Moreno-Manzano, Á. Serrano-Aroca, Graphene oxide nanosheets versus carbon nanofibers: enhancement of physical and biological properties of poly(3-hydroxybutyrate-co-3-hydroxyvalerate) films for biomedical applications, Int. J. Biol. Macromol. 143 (2020) 1000–1008, https://doi.org/10.1016/j.ijbiomac.2019.10.034.

[14] A.L. Rivera-Briso, Á. Serrano-Aroca, Poly(3-hydroxybutyrate-co-3-hydroxyvalerate): enhancement strategies for advanced applications, Polymers (Basel) 10 (2018) 732, https://doi.org/10.3390/polym10070732.

[15] A.L. Rivera-Briso, J.L. Aparicio-Collado, R.S.I. Serra, Á. Serrano-Aroca, Graphene oxide versus carbon nanofibers in poly(3-hydroxybutyrate-co-3-hydroxyvalerate) films: degradation in simulated intestinal environments, Polymers (Basel) 14 (2022) 348, https://doi.org/10.3390/polym14020348.

[16] P. Innocenzi, L. Stagi, Carbon-based antiviral nanomaterials: graphene, C-dots, and fullerenes. A perspective, Chem. Sci. 11 (2020) 6606–6622, https://doi.org/10.1039/d0sc02658a.

[17] S.H. Ku, M. Lee, C.B. Park, Carbon-based nanomaterials for tissue engineering, Adv. Healthc. Mater. 2 (2013) 244–260, https://doi.org/10.1002/adhm.201200307.

[18] J.L. Aparicio-Collado, J.J. Novoa, J. Molina-Mateo, C. Torregrosa-Cabanilles, Á. Serrano-Aroca, R.Sabater I. Serra, Novel semi-interpenetrated polymer networks of poly(3-hydroxybutyrate-co-3-hydroxyvalerate)/poly (vinyl alcohol) with incorporated conductive polypyrrole nanoparticles, Polym. 13 (2020) 57, https://doi.org/10.3390/POLYM13010057, 2021, Vol. 13, Page 57.

[19] S.H. Ku, M. Lee, C.B. Park, Carbon-based nanomaterials for tissue engineering, Adv. Healthc. Mater. 2 (2013) 244–260, https://doi.org/10.1002/adhm.201200307.

[20] J.L. Aparicio-Collado, N.García-San Martín, J. Molina-Mateo, C. Torregrosa Cabanilles, V.Donderis Quiles, A. Serrano-Aroca, R. Sabater i Serra, Electroactive calcium-alginate/polycaprolactone/reduced graphene oxide nanohybrid hydrogels for skeletal muscle tissue engineering, Colloids Surf. B Biointerfaces 112455 (2022), https://doi.org/10.1016/J.COLSURFB.2022.112455.

[21] S. Ullah, X. Chen, Fabrication, applications and challenges of natural biomaterials in tissue engineering, Appl. Mater. Today 20 (2020), https://doi.org/10.1016/j.apmt.2020.100656.

[22] Z. Jun, D. Guomin, Z. Mingzhu, P. Leilei, Z. Dagang, L. Rui, Crystallization and mechanical properties of reinforced PHBV composites using melt compounding: effect of CNCs and CNFs, Carbohydr. Polym. 168 (2017) 255–262.

[23] Q. Xue, X. Bin Liu, Y.H. Lao, L.P. Wu, D. Wang, Z.Q. Zuo, J.Y. Chen, J. Hou, Y. Y. Bei, X.F. Wu, K.W. Leong, H. Xiang, J. Han, Anti-infective biomaterials with surface-decorated tachyplesin I, Biomaterials 178 (2018) 351–362, https://doi.org/10.1016/j.biomaterials.2018.05.008.

[24] B.H.A. Rehm, M.F. Moradali, Alginates and Their Biomedical Applications, Springer Singapore, 2018, https://doi.org/10.1007/978-981-10-6910-9.

[25] G. Bickerstaff, J.E. Fraser, G.F. Bickerstaff, Entrapment in calcium alginate, Immobil. Enzym. Cells 1 (2003) 61–66, https://doi.org/10.1385/0-89603-386-4:61.

[26] C. Vilos, F.A. Morales, P.A. Solar, N.S. Herrera, F.D. Gonzalez-Nilo, D.A. Aguayo, H. L. Mendoza, J. Comer, M.L. Bravo, P.A. Gonzalez, S. Kato, M.A. Cuello, C. Alonso, E.J. Bravo, E.I. Bustamante, G.I. Owen, L.A. Velasquez, Paclitaxel-PHBV nanoparticles and their toxicity to endometrial and primary ovarian cancer cells, Biomaterials 34 (2013) 4098–4108, https://doi.org/10.1016/j.biomaterials.2013.02.034.

[27] M.L. Tebaldi, A.L.C. Maia, F. Poletto, F.V. de Andrade, D.C.F. Soares, Poly(-3-hydroxybutyrate-co-3-hydroxyvalerate) (PHBV): current advances in synthesis methodologies, antitumor applications and biocompatibility, J. Drug Deliv. Sci. Technol. 51 (2019) 115–126, https://doi.org/10.1016/j.jddst.2019.02.007.

[28] M.I. Idris, J. Zaloga, R. Detsch, J.A. Roether, H. Unterweger, C. Alexiou, A. R. Boccaccini, Surface modification of SPIONs in PHBV microspheres for biomedical applications, Sci. Rep. 8 (2018) 1–11, https://doi.org/10.1038/s41598-018-25243-9.

[29] S. Aznar-Cervantes, A. Pagán, J.G. Martínez, A. Bernabeu-Esclapez, T.F. Otero, L. Meseguer-Olmo, J.I. Paredes, J.L. Cenis, Electrospun silk fibroin scaffolds coated with reduced graphene promote neurite outgrowth of PC-12 cells under electrical stimulation, Mater. Sci. Eng. C 79 (2017) 315–325, https://doi.org/10.1016/j.msec.2017.05.055.

[30] Á. Serrano-Aroca, J.F.J.F. Ruiz-Pividal, M. Llorens-Gámez, Enhancement of water diffusion and compression performance of crosslinked alginate with a minuscule amount of graphene oxide, Sci. Rep. 7 (2017) 11684, https://doi.org/10.1038/s41598-017-10260-x.

[31] H. Andriamanantoanina, M. Rinaudo, Characterization of the alginates from five madagascan brown algae, Carbohydr. Polym. 82 (2010) 555–560, https://doi.org/10.1016/j.carbpol.2010.05.002.

[32] L. Cao, W. Lu, A. Mata, K. Nishinari, Y. Fang, Egg-box model-based gelation of alginate and pectin: a review, Carbohydr. Polym. 242 (2020), 116389, https://doi.org/10.1016/j.carbpol.2020.116389.

[33] B. Salesa, M. Llorens-Gámez, Á. Serrano-Aroca, Study of 1D and 2D carbon nanomaterial in alginate films, Nanomaterials 10 (2020) 206, https://doi.org/10.3390/nano10020206.

[34] Á. Serrano-Aroca, S. Deb, Synthesis of irregular graphene oxide tubes using green chemistry and their potential use as reinforcement materials for biomedical applications, PLoS One 12 (2017), e0185235, https://doi.org/10.1371/journal.pone.0185235.

[35] R. Guazzo, C. Gardin, G. Bellin, L. Sbricoli, L. Ferroni, F.S. Ludovichetti, A. Piattelli, I. Antoniac, E. Bressan, B. Zavan, Graphene-based nanomaterials for tissue engineering in the dental field, Nanomaterials 8 (2018) 1–31, https://doi.org/10.3390/nano8050349.

[36] W. Hooch Antink, Y. Choi, K.D. Seong, J.M. Kim, Y. Piao, Recent progress in porous graphene and reduced graphene oxide-based nanomaterials for electrochemical energy storage devices, Adv. Mater. Interfaces 5 (2018) 1–19, https://doi.org/10.1002/admi.201701212.

[37] M. Hu, Z. Yao, X. Wang, Graphene-based nanomaterials for catalysis, Ind. Eng. Chem. Res. 56 (2017) 3477–3502, https://doi.org/10.1021/acs.iecr.6b05048.

[38] Q. Zhang, Z. Wu, N. Li, Y. Pu, B. Wang, T. Zhang, J. Tao, Advanced review of graphene-based nanomaterials in drug delivery systems: synthesis, modification, toxicity and application, Mater. Sci. Eng. C 77 (2017) 1363–1375, https://doi.org/10.1016/j.msec.2017.03.196.

[39] B. Salesa, A. Tuñón-Molina, A. Cano-Vicent, M. Assis, J. Andrés, Á. Serrano-Aroca, Graphene nanoplatelets: in vivo and in vitro toxicity, cell proliferative activity, and cell gene expression, Appl. Sci. 12 (2022) 720, https://doi.org/10.3390/APP12020720, 2022, Vol. 12, Page 720.

[40] B. Frígols, M. Martí, B. Salesa, C. Hernández-Oliver, O. Aarstad, A.S.T. Ulset, G. I. Sætrom, F.L. Aachmann, Á. Serrano-Aroca, Graphene oxide in zinc alginate films: antibacterial activity, cytotoxicity, zinc release, water sorption/diffusion, wettability and opacity, PLoS One 14 (2019), https://doi.org/10.1371/journal.pone.0212819.

[41] B. Salesa, R.S.I. Serra, Á. Serrano-Aroca, Zinc chloride: time-dependent cytotoxicity, proliferation and promotion of glycoprotein synthesis and antioxidant

gene expression in human keratinocytes, Biology (Basel) 10 (2021) 1072, https://doi.org/10.3390/biology10111072.
[42] J.M. Silva, J.R. García, R.L. Reis, A.J. García, J.F. Mano, Tuning cell adhesive properties via layer-by-layer assembly of chitosan and alginate, Acta Biomater. 51 (2017) 279–293, https://doi.org/10.1016/j.actbio.2017.01.058.
[43] M. Martí, A. Tuñón-Molina, F.L. Aachmann, Y. Muramoto, T. Noda, K. Takayama, Á. Serrano-Aroca, Protective face mask filter capable of inactivating SARS-CoV-2, and methicillin-resistant Staphylococcus aureus and Staphylococcus epidermidis, Polymers (Basel) 13 (2021) 207, https://doi.org/10.3390/polym13020207.
[44] A. Cano-Vicent, A. Tuñón-Molina, M. Martí, Y. Muramoto, T. Noda, K. Takayama, Á. Serrano-Aroca, Antiviral face mask functionalized with solidified hand soap: low-cost infection prevention clothing against enveloped viruses such as SARS-CoV-2, ACS Omega (2021), https://doi.org/10.1021/acsomega.1c03511.
[45] A. Tuñón-Molina, M. Martí, Y. Muramoto, T. Noda, K. Takayama, Á. Serrano-Aroca, Antimicrobial face shield: next generation of facial protective equipment against SARS-CoV-2 and multidrug-resistant bacteria, Int. J. Mol. Sci. 22 (2021) 9518, https://doi.org/10.3390/IJMS22179518, 2021, Vol. 22, Page 9518.
[46] K. Takayama, A. Tuñón-Molina, A. Cano-Vicent, Y. Muramoto, T. Noda, J. L. Aparicio-Collado, R.S.i Serra, M. Martí, Á. Serrano-Aroca, Non-woven infection prevention fabrics coated with biobased cranberry extracts inactivate enveloped viruses such as SARS-CoV-2 and multidrug-resistant bacteria, Int. J. Mol. Sci. 22 (2021) 12719, https://doi.org/10.3390/ijms222312719.
[47] A. Tuñón-Molina, K. Takayama, E.M. Redwan, V.N. Uversky, J. Andrés, Á. Serrano-Aroca, Protective face masks: current status and future trends, ACS Appl. Mater. Interfaces 13 (48) (2021) 56725–56751, https://doi.org/10.1021/acsami.1c12227.
[48] A.M. Kropinski, A. Mazzocco, T.E. Waddell, E. Lingohr, R.P. Johnson, Enumeration of bacteriophages by double agar overlay plaque assay, Methods Mol. Biol. 501 (2009) 69–76, https://doi.org/10.1007/978-1-60327-164-6_7.
[49] Total RNA Purification Kit Product Insert, (n.d.).
[50] S. Il Park, Y. Zhao, Incorporation of a high concentration of mineral or vitamin into chitosan-based films, J. Agric. Food Chem. 52 (2004) 1933–1939, https://doi.org/10.1021/jf034612p.
[51] M. Llorens-Gámez, Á. Serrano-Aroca, Low-cost advanced hydrogels of calcium alginate/carbon nanofibers with enhancedwater diffusion and compression properties, Polymers (Basel) 10 (2018), https://doi.org/10.3390/polym10040405.
[52] J.K. Wassei, R.B. Kaner, Graphene, a promising transparent conductor, Mater. Today 13 (2010) 52–59, https://doi.org/10.1016/S1369-7021(10)70034-1.
[53] Z. Lin, X. Ye, J. Han, Q. Chen, P. Fan, H. Zhang, D. Xie, H. Zhu, M. Zhong, Precise control of the number of layers of graphene by picosecond laser thinning, Sci. Rep. 5 (2015) 11662.
[54] D. Chen, H. Zhu, T. Liu, In situ thermal preparation of polyimide nanocomposite films containing functionalized graphene sheets, ACS Appl. Mater. Interfaces 2 (2010) 3702–3708, https://doi.org/10.1021/AM1008437/SUPPL_FILE/AM1008437_SI_001.PDF.
[55] S. Muniyasamy, O. Ofosu, B. Thulasinathan, A.S. Thondi Rajan, S.M. Ramu, S. Soorangkattan, J.B. Muthuramalingam, A. Alagarsamy, Thermal-chemical and biodegradation behaviour of alginic acid treated flax fibres/ poly(hydroxybutyrate-co-valerate) PHBV green composites in compost medium, Biocatal. Agric. Biotechnol. 22 (2019), 101394, https://doi.org/10.1016/j.bcab.2019.101394.
[56] P. Sanz-Ruiz, E. Carbó-Laso, J.C. Del Real-Romero, F. Arán-Ais, Y. Ballesteros-Iglesias, E. Paz-Jiménez, M. Sánchez-Navarro, M.Á. Pérez-Limiñana, J. Vaquero-Martín, Microencapsulation of rifampicin: a technique to preserve the mechanical properties of bone cement, J. Orthop. Res. 36 (2018) 459–466, https://doi.org/10.1002/jor.23614.
[57] L. Rezaie Shirmard, M. Ghofrani, N. Bahari Javan, S. Bayrami, A. Tavassoli, A. Rezaie, M. Amini, A. Kebriaee-zadeh, M.R. Rouini, R. Dinarvand, M. Rafiee-Tehrani, F.A. Dorkoosh, Improving the in-vivo biological activity of fingolimod loaded PHBV nanoparticles by using hydrophobically modified alginate, Drug Dev. Ind. Pharm. 46 (2020) 318–328, https://doi.org/10.1080/03639045.2020.1721524.
[58] M.J. Costa, A.M. Marques, L.M. Pastrana, M. Sillankorva, M.A. Cerqueira, A. M. Marques, L.M. Pastrana, S.M. Sillankorva, M.A. Cerqueira, Accepted Manuscript, 2018, https://doi.org/10.1016/j.foodhyd.2018.03.014.
[59] M. Martí, B. Frígols, B. Salesa, Á. Serrano-Aroca, Calcium alginate/graphene oxide films: reinforced composites able to prevent Staphylococcus aureus and methicillin-resistant Staphylococcus epidermidis infections with no cytotoxicity for human keratinocyte HaCaT cells, Eur. Polym. J. 110 (2019), https://doi.org/10.1016/j.eurpolymj.2018.11.012.
[60] A.L. Rivera-Briso, F.L. Aachmann, V. Moreno-Manzano, Á. Serrano-Aroca, Graphene oxide nanosheets versus carbon nanofibers: enhancement of physical and biological properties of poly(3-hydroxybutyrate-co-3-hydroxyvalerate) films for biomedical applications, Int. J. Biol. Macromol. 143 (2020) 1000–1008, https://doi.org/10.1016/j.ijbiomac.2019.10.034. In press.
[61] D. Baltimore, Expression of animal virus genomes, Bacteriol. Rev. 35 (1971) 235–241, https://doi.org/10.1128/mmbr.35.3.235-241.1971.
[62] Á. Serrano-Aroca, Antiviral characterization of advanced materials: use of bacteriophage Phi 6 as surrogate of enveloped viruses such as SARS-CoV-2, Int. J. Mol. Sci. 23 (2022) 5335, https://doi.org/10.3390/IJMS23105335.
[63] A.M. Díez-Pascual, State of the art in the antibacterial and antiviral applications of carbon-based polymeric nanocomposites, Int. J. Mol. Sci. 22 (2021) 10511, https://doi.org/10.3390/ijms221910511.
[64] J.P. Vallejo, U. Calviño, I. Freire, J. Fernández-Seara, L. Lugo, Convective heat transfer in pipe flow for glycolated water-based carbon nanofluids. A thorough analysis, J. Mol. Liq. 301 (2020), 112370, https://doi.org/10.1016/j.molliq.2019.112370.
[65] Á. Serrano-Aroca, L. Iskandar, S. Deb, Green synthetic routes to alginate-graphene oxide composite hydrogels with enhanced physical properties for bioengineering applications, Eur. Polym. J. 103 (2018) 198–206, https://doi.org/10.1016/j.eurpolymj.2018.04.015.
[66] E.I. Paşcu, J. Stokes, G.B. McGuinness, Electrospun composites of PHBV, silk fibroin and nano-hydroxyapatite for bone tissue engineering, Mater. Sci. Eng. C 33 (2013) 4905–4916, https://doi.org/10.1016/j.msec.2013.08.012.
[67] B. Fei, C. Chen, H. Wu, S. Peng, X. Wang, L. Dong, Quantitative FTIR study of PHBV/bisphenol A blends, Eur. Polym. J. 39 (2003) 1939–1946, https://doi.org/10.1016/S0014-3057(03)00114-9.
[68] M. Rashtchian, A. Hivechi, S.H. Bahrami, P.B. Milan, S. Simorgh, Fabricating alginate/poly(caprolactone) nanofibers with enhanced bio-mechanical properties via cellulose nanocrystal incorporation, Carbohydr. Polym. 233 (2020), 115873, https://doi.org/10.1016/j.carbpol.2020.115873.
[69] C. Xiao, L. Weng, L. Zhang, Improvement of physical properties of crosslinked alginate and carboxymethyl konjac glucomannan blend films, J. Appl. Polym. Sci. 84 (2002) 2554–2560, https://doi.org/10.1002/app.10582.
[70] T.S. Pathak, J.H. Yun, J. Lee, K.J. Paeng, Effect of calcium ion (cross-linker) concentration on porosity, surface morphology and thermal behavior of calcium alginates prepared from algae (Undaria pinnatifida), Carbohydr. Polym. 81 (2010) 633–639, https://doi.org/10.1016/j.carbpol.2010.03.025.
[71] V. Ţucureanu, A. Matei, A.M. Avram, FTIR spectroscopy for carbon family study, Crit. Rev. Anal. Chem. 46 (2016) 502–520, https://doi.org/10.1080/10408347.2016.1157013.
[72] S. Rao, J. Upadhyay, K. Polychronopoulou, R. Umer, R. Das, Reduced graphene oxide: effect of reduction on electrical conductivity, J. Compos. Sci. 2 (2018), https://doi.org/10.3390/jcs2020025.
[73] S. Singh, A.K. Mohanty, Wood fiber reinforced bacterial bioplastic composites: fabrication and performance evaluation, Compos. Sci. Technol. 67 (2007) 1753–1763, https://doi.org/10.1016/j.compscitech.2006.11.009.
[74] Q.S. Liu, M.F. Zhu, W.H. Wu, Z.Y. Qin, Reducing the formation of six-membered ring ester during thermal degradation of biodegradable PHBV to enhance its thermal stability, Polym. Degrad. Stab. 94 (2009) 18–24, https://doi.org/10.1016/j.polymdegradstab. 2008.10.016.
[75] R. Sabater i Serra, J. Molina-mateo, C. Torregrosa-cabanilles, A. Andrio-Balado, J. Meseguer Dueñas, A. Serrano-Aroca, Bio-nanocomposite hydrogel based on zinc conformation , thermal behavior / degradation , and dielectric properties, Polymers (Basel) 12 (2020) 702.
[76] H. Kim, A.A. Abdala, C.W. MacOsko, Graphene/polymer nanocomposites, Macromolecules 43 (2010) 6515–6530, https://doi.org/10.1021/ma100572e.
[77] M. El Achaby, F.-E. Arrakhiz, S. Vaudreuil, A. el Kacem Qaiss, M. Bousmina, O. Fassi-Fehri, Mechanical, thermal, and rheological properties of graphene-based polypropylene nanocomposites prepared by melt mixing mounir, Polym. Compos. 33 (2012) 733–744, https://doi.org/10.1002/pc.22198.
[78] P. Laurienzo, M. Malinconico, A. Motta, A. Vicinanza, Synthesis and characterization of a novel alginate-poly(ethylene glycol) graft copolymer, Carbohydr. Polym. 62 (2005) 274–282, https://doi.org/10.1016/j.carbpol.2005.08.005.
[79] A.S. El-Houssiny, A.A. Ward, D.M. Mostafa, S.L. Abd-El-Messieh, K.N. Abdel-Nour, M.M. Darwish, W.A. Khalil, Drug-polymer interaction between glucosamine sulfate and alginate nanoparticles: FTIR, DSC and dielectric spectroscopy studies, Adv. Nat. Sci. Nanosci. Nanotechnol. 7 (2016), 025014, https://doi.org/10.1088/2043-6262/7/2/025014.
[80] R. Requena, A. Jiménez, M. Vargas, A. Chiralt, Effect of plasticizers on thermal and physical properties of compression-moulded poly[(3-hydroxybutyrate)-co-(3-hydroxyvalerate)] films, Polym. Test. 56 (2016) 45–53, https://doi.org/10.1016/j.polymertesting.2016.09.022.
[81] B. Alemour, M.H. Yaacob, H.N. Lim, M.R. Hassan, Review of electrical properties of graphene conductive composites, Int. J. Nanoelectron. Mater. 11 (2018) 371–398.
[82] G. Kaur, R. Adhikari, P. Cass, M. Bown, P. Gunatillake, Electrically conductive polymers and composites for biomedical applications, RSC Adv. 5 (2015) 37553–37567, https://doi.org/10.1039/c5ra01851j.
[83] V.B. Mohan, B.J. Krebs, D. Bhattacharyya, Development of novel highly conductive 3D printable hybrid polymer-graphene composites, Mater. Today Commun. 17 (2018) 554–561, https://doi.org/10.1016/j.mtcomm.2018.09.023.
[84] A.S. Wajid, S. Das, F. Irin, H.S.T. Ahmed, J.L. Shelburne, D. Parviz, R.J. Fullerton, A.F. Jankowski, R.C. Hedden, M.J. Green, Polymer-stabilized graphene dispersions at high concentrations in organic solvents for composite production, Carbon N. Y. 50 (2012) 526–534, https://doi.org/10.1016/j.carbon.2011.09.008.
[85] F. Jakubka, S.P. Schießl, S. Martin, J.M. Englert, F. Hauke, A. Hirsch, J. Zaumseil, Effect of polymer molecular weight and solution parameters on selective dispersion of single-walled carbon nanotubes, ACS Macro Lett. 1 (2012) 815–819, https://doi.org/10.1021/mz300147g.
[86] D.W. Johnson, B.P. Dobson, K.S. Coleman, A manufacturing perspective on graphene dispersions, Curr. Opin. Colloid Interface Sci. 20 (2015) 367–382, https://doi.org/10.1016/j.cocis.2015.11.004.